# DISCOVERING CLONE NEGATIVES VIA ADAPTIVE CONTRASTIVE LEARNING FOR IMAGE-TEXT MATCHING

**Anonymous authors**
Paper under double-blind review

## ABSTRACT

In this paper, we identify a common yet challenging issue in image-text matching, i.e., clone negatives: negative image-text pairs that are semantic-consistent with the positives, which leads to ambiguous and suboptimal matching results. To address this, we propose Adaptive Contrastive Learning (AdaCL), which introduces two margin parameters with a modulating anchor to dynamically strengthen the compactness between positives and mitigating the impact of clone negatives. The modulating anchor is selected based on the distribution of negative samples without explicit training, allowing for progressive tuning and enhanced in-batch supervision. Extensive experiments on image-text matching, CLIP pre-training, and text-based person search demonstrate the superiority of AdaCL in image-text matching and contrastive image-text pretraining. Furthermore, we extend AdaCL to weakly-supervised image-text matching by substituting human-annotated descriptions with automatically generated captions, increasing the number of potential clone negatives. AdaCL demonstrates robustness with the generated captions, alleviating the reliance on crowd-sourced annotations and laying a foundation for scalable vision-language contrastive learning.

## 1 INTRODUCTION

Image-text matching(Fang et al., 2023; Bin et al., 2023; Qu et al., 2021; Huang et al., 2019; Shi et al., 2019; Chen et al., 2021) has become de facto the most fundamental multimodal task in recent years, which involves searching for images with text queries (text-image) and the retrieval of sentences using images (image-text).

Existing image-text matching methods usually learn a robust cross-modal representation through various fusion paradigms, such as object-level or global-level aligning(Bin et al., 2023; Zhang et al., 2022; Wang et al., 2022a; Cheng et al., 2022; Li et al., 2022b; Qu et al., 2021; Chen et al., 2021; Wang et al., 2020a; Wu et al., 2019; Li et al., 2019; Lee et al., 2018). On the other hand, contrastive learning(Li et al., 2022a; Radford et al., 2021; He et al., 2020; Oord et al., 2018; Zhang & Lu, 2018) has been widely adopted as the objective, which brings similar (or positive) samples closer in the latent space while pushing dissimilar (or negative) samples apart. Among them, Triplet ranking loss (TRL)(Wang et al., 2019; 2018; Faghri et al., 2017) and Contrastive loss (CL)(Li et al., 2021; Radford et al., 2021; He et al., 2020) have witnessed the success of vision-language contrastive learning. Specifically, TRL preserves the relative distance between in-batch samples through a manually-set fixed margin. CL is defined as the cross-entropy of the softmax-normalized similarity between each image-text pair. In self-supervised learning and multimodal learning, InfoNCE and its variants Cheng et al. (2020); Oord et al. (2018); Ma & Collins (2018); Liang et al. (2024); Cheng et al. (2020); Zhang & Lu (2018) are the prevalent forms of CL.

Despite these advancements, current contrastive learning for image-text matching faces an inherent challenge: During an in-batch learning, it is common for image-text pairs to possess semantically related text annotations and similar visual cues, thereby rendering them practically indistinguishable (reflected by their closing similarity scores). As shown in Figure 1(a), $T_2$ is a typical hard negative for $I_1$, which has been widely discussed (Pan et al., 2023a; Wang et al., 2020b; Zhang et al., 2022). It is noteworthy that apart from the key semantic "two skyscrapers", $T_3$ is semantically-consistent with $I_1$. Although matching $I_1$ and $T_3$ is indeed correct, it is no doubt a **suboptimal** result because the ground-truth annotation $T_1$ exhibits more precise and fine-grained semantics, demonstrating a

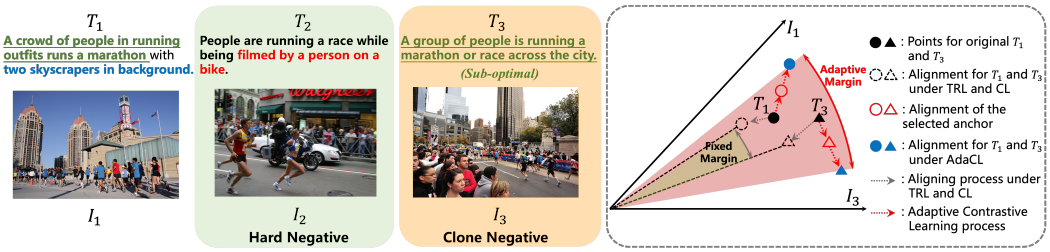


(a) Observational issue: Clone negatives (b) Geometrical illustration

Figure 1: (a) An example of "hard negatives" and "clone negatives", Compared with the gold label ($T_1$), the clone negative ($T_3$) is defined as a "sub-optimal" text sample. (b) Geometrical illustration of the proposed Adaptive Contrastive Learning, which adaptively enlarges the distance between positives and clone negatives.

closer correspondence with $I_1$. Different from false negatives which should be considered as "true", we refer to samples like $T_3$ as ***clone negatives***, which is quite challenging for matching in such scenarios. Distinguishing clone negatives through cross-modal fusion is highly intractable since clone negatives are also "positive". Also, existing contrastive learning primarily focuses on negative mining strategies for single modality (Wang et al., 2024; Robinson et al., 2020; Guo et al., 2022; Yang et al., 2021), or learning noise correspondence (Han et al., 2024; Huang et al., 2021). Image-text matching continues to predominantly rely on vanilla TRL or CL as the learning objective, which set a fixed margin during training, making it tough to actively address the issue of clone negatives since it has already pre-defined the label of all the image-text pairs (positive or negative).

In this work, we propose Adaptive Contrastive Learning (AdaCL) to exploit reliable clone negatives and distinguish them effectively in image-text matching. Instead of the fixed learning pattern of TRL and CL, we specifically add two margin parameters, serving as scaling and shifting factors, to synchronously enhance the compactness of positives while introducing the supervision of the clone negatives. To progressively tune the margin parameters, we propose to select a modulating *anchor* from each in-batch similarity score based on Gaussian discriminant analysis without explicit training. In this way, *anchor* effectively reflects the intensity of in-batch clone negatives, and imposes a more substantial penalty through the margin parameters, thereby adaptively enlarging the distance between positives and clone negatives. Comprehensive experiments conducted on image-text matching (Flickr30K and MS-COCO), CLIP pre-training (CC3M and CC12M), and text-based person search (CUHK-PEDES, ICFG-PEDES, RSTPReid) demonstrate the effectiveness and robustness of AdaCL.

Moreover, AdaCL can be applied to weakly-supervised image-text matching with *structured and standardized text annotations*. We propose to increase the number of potential clone negatives by substituting the original textual descriptions with automatically generated captions using image captioning methods. We verify AdaCL by four distinct captioning tools, and it is observed that AdaCL can also learn robust cross-modal semantics. This not only demonstrates the superiority of AdaCL in distinguishing clone negatives, but also mitigating the need of crowd-sourcing annotations, laying a foundation for future vision-language contrastive learning.

To sum up, the main contributions of this paper can be summarized as follows.

- We elucidate the issue of ***clone negatives***: semantic-consistent but suboptimal matching candidates, and highlight the challenge they pose to existing contrastive learning for image-text matching.
- We propose Adaptive Contrastive Learning (AdaCL), introducing two margin parameters that dynamically propagates the semantics of clone negatives during training, enhancing the compactness of positives and mitigating the impact of clone negatives.
- AdaCL demonstrates superiority in both supervised and weakly-supervised image-text matching, which use automatically generated captions as annotations. Extensive experiments prove the robustness of AdaCL, alleviating the reliance on manual annotations.

## 2 RELATED WORK

**Image-Text Matching.** The general process of Image-text matching can be attributed to two key components: (1) cross-modal feature fusion, and (2) learning objectives. The former can be categorized to global representation fusion and region-level fragment fusion. Global representation fusion extracts holistic feature from two modalities, and then mapping them to a joint visual-textual alignment where the similarity is calculated(Zhang & Lu, 2018; Ma et al., 2015). Region-level fragment fusion captures local content of two modalities to enhance the cross-modal interaction(Li et al., 2017a; Lee et al., 2018; Cheng et al., 2022; Diao et al., 2021). Apart from this, graph-structured methods (Liu et al., 2020; Wang et al., 2020a; Li et al., 2022b) also leverage nodes to represent region-level matching, further exploiting the instance relationships. The learning objectives of image-text matching can be categorized to contrastive loss (CL) (Li et al., 2022a; Radford et al., 2021; He et al., 2020; Oord et al., 2018; Zhang & Lu, 2018) and triplet ranking loss (TRL) (Wang et al., 2019; 2018). For CL, Zhang & Lu (2018); Wang et al. (2020b) proposed to minimize the distance between the projection distributions and the normalized matching distributions together with a classification objective. TRL is widely adpoted by existing image-text matching methods based on unique network designing (Wang et al., 2018; Pan et al., 2023a; Qu et al., 2021). Several studies have sought to address false negatives by reducing sampling weights(Li et al., 2023a; Zhang et al., 2022; Li et al., 2023c), which is essentially a "passive" approach. However, such methods cannot handle clone negatives due to the fundamental differences between false negatives and clone negatives, as the former often carry high learning value. Also, both TRL and CL are inherently limited by a manully-set margin, which fails to consider the sample discrepancy of clone negatives. To address this challenge, a pivotal solution lies a learning objective capable of adaptively modulating the margin.

**Contrastive Learning.** Contrastive learning has emerged as a powerful paradigm in self-supervised learning and representation learning, aiming to learn discriminative features by contrasting positive pairs against negative pairs (Schroff et al., 2015; Oord et al., 2018; Zhang & Lu, 2018). The foundation of contrastive learning can be traced back to metric learning, where the goal was to learn a distance function that better represents the underlying structure of the data (Bromley et al., 1993; Taigman et al., 2014; Wang et al., 2017; Grill et al., 2020; Caron et al., 2020). Seminal works such as SimCLR (Chen et al., 2020b) and MoCo (He et al., 2020) established the foundation for contrastive learning in computer vision. The former introduced a simple yet effective approach using data augmentation and a large batch size, while the latter proposed a momentum encoder to maintain a consistent dictionary of negative samples. In parallel to its success in computer vision, contrastive learning has also shown promise in multimodal learning (Radford et al., 2021; Li et al., 2022a; 2021), which employed a contrastive objective to align text and image representations in a shared latent space. By pretraining on large-scale text-image pairs, remarkable zero-shot transfer capabilities can be achieved. Despite its success, the requirement for high-quality datasets is still a significant hurdle for many applications. Real world scenarios are filled with clone negatives, which hinder a broader adoption of contrastive learning.

## 3 ADAPTIVE CONTRASTIVE LEARNING

Our aim is to synchronously enhance the compactness between positive samples and calibrating the supervision of clone negatives. We begin by revisiting vanilla contrastive learning, followed by our proposed Adaptive Contrastive Learning (AdaCL) and the anchor selection methdology. By replacing TRL and CL with AdaCL, both the matching performance and robustness have been greatly improved, demonstrated by supervised and weakly-supervised image-text matching on various baselines.

### 3.1 PRELIMINARIES

**Architecture of contrastive learning**. The prerequisites for vision-language contrastive learning include textual and visual modalities. Given a text description with $a$ words and the pairwise image, the textual backbone are denoted as $\mathcal{F}_t(\cdot)$. Each word vector is mapped to the common space through a fully connected layer. The visual backbone is denoted as $\mathcal{F}_v(\cdot)$, which generates a sequence of $n$ patches to exploit the original semantics of the image. The fine-grained representation of both modalities can be denoted as: $\mathbf{w} = \mathcal{F}_t(T) \in \mathbb{R}^{a \times D_t}$ and $\mathbf{v} = \mathcal{F}_v(I) \in \mathbb{R}^{n \times D_v}$. The similarity score of a certain image-text pair can be denoted as $s(I, T) = g_v(\mathbf{v})^{\mathsf{T}} g_w(\mathbf{w})$. For clarity and readability,

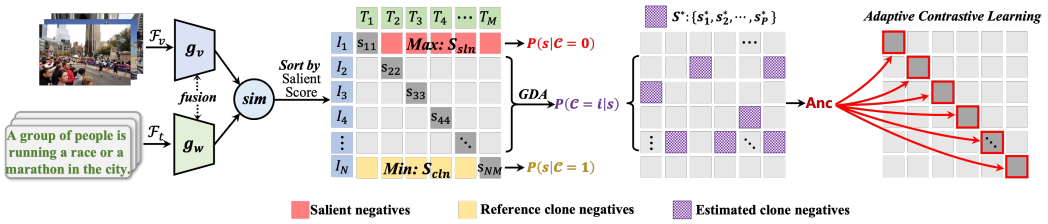


Figure 2: Illustration of Adaptive Contrastive Learning (AdaCL). Salient negatives and Reference clone negatives are selected by Salient Score (Sec. 3.3). AdaCL dynamically adjusts two introduced margin parameters based on a Gaussian discriminant analysis of clone negatives, enabling a more refined contrastive learning objective. This approach progressively tunes the margins to effectively regulate the distance between positives and clone negatives (Sec. 3.2). Unlike traditional contrastive learning methods, AdaCL adapts its parameters to the intensity of clone negatives, enhancing robustness in challenging scenarios. Additionally, AdaCL features a plug-and-play design, demonstrating excellent adaptability and compatibility across various tasks (Sec. 4).

we use $g_v(\cdot)$ and $g_w(\cdot)$ to represent optional cross-modal operations (such as fusion or connector) between visual and textual representation, where $D$ is the dimension of the joint embedding space.

**Training objective.** The training objective of current contrastive learning rely on a fixed learning pattern to narrow the distance between positive samples. Specifically, the softmax normalized similarity for image $I$ and its corresponding text $T_i$ can be denoted as:

$$p_i(I) = \frac{\exp(s(I, T_i)/\tau)}{\sum_{j=1}^{M+1} \exp(s(I, T_j)/\tau)}, \tag{1}$$

where the denominator $M+1$ consists of one positive and $M$ negatives. It is noteworthy that if momentum memory bank is not used, then $M$ equals to the mini-batch size $N$. $\tau$ is a fixed temperature parameter controlling the overall supervision. $p_i(I)$ represents the probability of assigning $I$ to the corresponding ground truth $T_i$. Then, a cross-entropy loss is employed, which can be expressed as:

$$\mathcal{L} = \mathbb{E}_{I\sim D}\left[\mathbb{H}(\mathbf{y}(I), \mathbf{p}(I))\right] = -\frac{1}{N}\sum_{i=1}^{N} y_i(I)\log(p_i(I)), \tag{2}$$

where $\mathbf{y}(I)$ is a one-hot distribution where the ground-truth is set by 1. Equation 2 pulls closer positive image-text pairs while pushing away the *pre-defined* negative pairs.

### 3.2 Adaptive Contrastive Learning

Current image-text matching typically utilize TRL(Wang et al., 2019; 2018) and CL(Zhang & Lu, 2018; Wang et al., 2020b; Radford et al., 2021) during training. However, as mentioned before, it is highly intractable to distinguish clone negatives, leading to insufficient cross-modal representation. Also, the semantic discrepancy between positives and clone negatives cannot be fully exploited. Based on this fact, we propose AdaCL by introducing two margin parameters that play the role of scaling and shifting factors. The margin parameters are adaptively tuned under the supervision of potential clone negatives selected via the distribution of in-batch similarity logits.

For simplicity, we analyze the $i$-th image-text pair from a mini-batch. In order to uncover and enhance the supervision of potential clone negatives, we introduce two margin parameters to $p_i(I)$ to serve as the scaling and shifting factors:

$$\hat{p}_i(I) = \frac{\exp\left[m_1(s(I, T_i) - m_2)\right]}{\exp\left[m_1(s(I, T_i) - m_2)\right] + \sum_{j-1, j\neq i}^{M+1} \exp\left[s(I, T_j)\right]}, \tag{3}$$

$m_1$ and $m_2$ are the tuning targets during training. For the tuning process, we strategically select a specific *anchor* that embodies the characteristics of clone negatives. *anchor* serves as a regulation in the overall supervision of in-batch clone negatives (details in Section 3.3). In order to compute $m_1$ and $m_2$ during each batch learning, two conditions are specifically analyzed. (1) First, the probability of *anchor* can be obtained using Equation 3:

$$\hat{p}_u = \frac{\exp\left[m_1(anchor - m_2)\right]}{\exp\left[m_1(anchor - m_2)\right] + \sum_{anchor}}, \tag{4}$$

where $\sum_{anchor}$ is the simplification of $\sum_{k=1,k\neq u}^{M+1} \exp\left[s(I_u, T_k)\right]$. Since *anchor* represents the ensemble average probability of potential in-batch clone negatives, its corresponding $\hat{p}_u$ reflects the approximate convergence degree of the model to a large extent. (2) Second, if we can control the probability of $\hat{p}_u$, then the overall supervision within the mini-batch are well regulated. Therefore, we propose to progressively tune $m_1$ and $m_2$ based on $\hat{p}_u$. To achieve this, a specific boundary condition of Equation 4 is analyzed: Since cross-entropy loss is represented as $L = -log(\hat{p}_u)$, when the score of *anchor* $s(I_u, T_u)$ (equals to $s^{pos}$ in Equation 11) approaches 1 (indicating a high similarity), a relative small $m_1$ would unnecessarily penalize the loss function for correct image-text pairs. Based on this fact, we reason out a condition that $\hat{p}_u$ should be as close to 1 as possible when $s(I_u, T_u)$ approaches 1, to boost distinguishing clone negatives. This condition can be denoted as:

$$\lim_{s(I_u,T_u)\to 1} \hat{p}_u \approx 1. \tag{5}$$

Combining Equation 4, we can approximate the following boundary:

$$\frac{\exp\left[m_1(1 - m_2)\right]}{\exp\left[m_1(1 - m_2)\right] + \sum_{anchor}} = 1 - \epsilon, \tag{6}$$

where $\epsilon$ is a small value added to avoid $m_1$ reaches 0. With Equation 4 and Equation 6, we can derive the values of $m_1$ and $m_2$ in Equation 3 iteratively and update $\mathcal{L}_{ada}$ based on the objective format in Equation 2 during training. In this way, $\mathcal{L}_{ada}$ effectively propagates the semantics of clone negatives via $m_1$ and $m_2$. The detailed derivation is in A.3 of the appendix.

### 3.3 Anchor Selection

As mentioned above, our aim is to select a salient *anchor* from the in-batch similarity scores to control the supervision of potential clone negatives. It is intuitive that the image/text with the highest similarity score with its positive text/image is more likely to be an salient negative, while a relatively lower score corresponds to a potential negative which is hard to distinguish. To best quantitatively analyze the in-batch similarity, we introduce a Salient Score for anchor selection. Specifically, $S_i = \{s_{ij}\}_{j=1}^{M+1}$ refers to the similarity between each in-batch text/image and the $i^{th}$ image/text, and $s_{ii}$ is the positive. Then, the salient score of each in-batch sample is defined as the difference between the positive and the average similarity of the negatives. Mathematically, it can be expressed as:

$$\text{Salient Score}_i = s_{ii} - \frac{1}{M} \sum_{j=1,j\neq i}^{M+1} s_{ij}. \tag{7}$$

Compared with directly choosing the sample with the highest similarity, salient score better reflects the "salient" extent by considering the negative similarity. We select the image-text pair with the highest salient score as $S_{sln}$, which represents 1 positive and $M$ salient negatives. On the contrary, the image-text pair with the lowest salient score is $S_{cln}$, which consists of 1 positive and $M$ potential clone negatives.

To predict the potential clone negatives from each mini-batch, a straightforward and simple way is to calculate the salient score of the rest in-batch image-text pairs. However, we found that in contrastive learning, similarity scores typically do not exhibit significant numerical differences, thus applying salient score to all the samples may result in over-fitting. Therefore, we revisit and propose to use a classical algorithm, i.e., Gaussian Discriminant Analysis (GDA) for training-free prediction. GDA allows for the exploitation of clone negatives **without** the need for explicit training. Specifically, the classification probability can be formulated as follows:

$$p\left(\mathcal{C} \mid s\right) = \frac{p\left(s \mid \mathcal{C}\right) p\left(\mathcal{C}\right)}{p\left(s \mid \mathcal{C}\right) p\left(\mathcal{C}\right) + p\left(s \mid \bar{\mathcal{C}}\right) p\left(\bar{\mathcal{C}}\right)} = \frac{\exp\left(a_c\right)}{\exp\left(a_c\right) + \exp\left(a_{\bar{c}}\right)}. \tag{8}$$

Here a binary classification is adopted, thus $\mathcal{C}$ and $\bar{\mathcal{C}}$ represent the pairwise similarity is / is not a clone negative respectively. $s$ is the similarity score. The logit function is $a_c = \log(p(s \mid \mathcal{C})p(\mathcal{C}))$.

Therefore, the classifier can be obtained by analyzing the data distribution of clone negatives and its prior distribution. In GDA, the features are typically assumed to follow the Gaussian distribution with identical covariance. Since the dimension of similarity score is 1, i.e., $s \in \mathbb{R}$, the aforementioned distribution expression can be simplified to a univariate distribution, where $(s \mid \bar{\mathcal{C}}) \sim \mathcal{N}\left(\mu_0, \sigma_0^2\right)$, and $(s \mid \mathcal{C}) \sim \mathcal{N}\left(\mu_1, \sigma_1^2\right)$ Combining this assumption to Equation 8, we can obtain:

$$p\left(\mathcal{C} \mid s\right) = \frac{1}{1 + \frac{\pi_0}{\pi_1}\frac{\sigma_1}{\sigma_0}\exp\left[\frac{(s-\mu_1)^2}{2\sigma_1^2} - \frac{(s-\mu_0)^2}{2\sigma_0^2}\right]}, \tag{9}$$

where $\pi_c$ and $\pi_{\bar{c}}$ are the priors of $\mathcal{C}$ and $\bar{\mathcal{C}}$ respectively. Given that $S_{sln}$ and $S_{cln}$ comprise the most representative salient negatives and potential clone negatives within a mini-batch, we utilize the negatives from $S_{sln}$ and $S_{cln}$ within each mini-batch to represent the empirical means and variances $\mu_c$, $\mu_{\bar{c}}$, $\sigma_c$, and $\sigma_{\bar{c}}$. The potential in-batch clone negatives are selected based on the criterion:

$$S^* := \{s \mid p\left(\mathcal{C} \mid s\right) > p\left(\bar{\mathcal{C}} \mid s\right)\}, \tag{10}$$

where $S^*$ is the estimated clone negative set from a mini-batch. Finally, *anchor* is obtained by the median of $\Delta S$, which is defined as follows:

$$\Delta S = \{\delta \mid \delta = |s^{pos} - s|\}, \forall s \in S^*;\ \textit{anchor} := s^{pos} \mid \delta = \text{median}(\Delta S). \tag{11}$$

*anchor* reflects the average discrepancy between all potential clone negatives and their corresponding positive. With *anchor* and adaptive contrastive learning in Section 3.2, the overall process of AdaCL is expressed in Algorithm 1.

**Algorithm 1** Adaptive Contrastive Learning

**Input:** a mini-batch of $N$ image-text pairs, with $N$ positives and $N \cdot M$ negatives.
**Output:** $\mathcal{L}_{ada}$

1: **for** each mini-batch **do**
2: Select in-batch grounding salient negatives and clone negatives;
$S_{sln} = \{s_{i^+j}\} \mid j \in M, i^+ = \text{argmax}_i \text{ Salient Score}_i$,
$S_{cln} = \{s_{i^-j}\} \mid j \in M, i^- = \text{argmin}_i \text{ Salient Score}_i$,
3: Sort out in-batch potential clone negatives $S^*$, and select *anchor* based on $\Delta S$;
$p\left(\mathcal{C} \mid s\right) = 1/\{1 + \frac{\pi_0}{\pi_1}\frac{\sigma_1}{\sigma_0}\exp\left[\frac{(s-\mu_1)^2}{2\sigma_1^2} - \frac{(s-\mu_0)^2}{2\sigma_0^2}\right]\}$,
$S^* := \{s \mid p\left(\mathcal{C} = 1 \mid s\right) > p\left(\mathcal{C} = 0 \mid s\right)\}$, $\textit{anchor} := s^{pos} \mid \delta = \text{median}(\Delta S)$,
4: Obtain the probability of *anchor* for tuning;
$\hat{p}_u = \frac{\exp[m_1(\textit{anchor} - m_2)]}{\exp[m_1(\textit{anchor} - m_2)] + \sum_{\textit{anchor}}}$,
5: Compute $m_1$ and $m_2$ according to Eq. 4 and Eq. 6;
$m_1 = log(\frac{\epsilon\ \hat{p}_u}{(1-\epsilon)(1-\hat{p}_u)})/(\textit{anchor} - 1),\ m_2 = \textit{anchor} + log(\frac{1-\hat{p}_u}{\hat{p}_u\ \sum_{\textit{anchor}}})/m_1$;
6: Update $\hat{p}_i(I)$ and $\mathcal{L}_{ada}$;
$\hat{p}_i(I) = \frac{\exp[m_1(s(I,T_i) - m_2)]}{\exp[m_1(s(I,T_i) - m_2)] + \sum_{j-1, j\neq i}^{M+1}\exp[s(I,T_j)]}$, $\mathcal{L}_{ada} = \mathbb{E}_{I\sim D}\left[\mathbb{H}(\mathbf{y}(I), \hat{\mathbf{p}}(I))\right]$.
7: **end for**

### 3.4 Weakly-supervised Matching with Pseudo Captions

Existing image-text datasets typically consist of detailed text descriptions to comprehensively cover fine-grained representations that appear in the corresponding images. However, in practical applications, image-text pairs are mainly scraped from the Internet. These raw datasets not only contain inherent noises but also exhibit a ***high degree of correlation***: for two semantic-distinct images, their corresponding text descriptions may be semantic-consistent. This intrinsic characteristic has been largely overlooked in existing benchmarks. Moreover, research trend has recently been shifting towards prompt-based semi-automatic annotations, which is totally different from current image-text dataset format.

To validate the applicability of AdaCL in ***a more general annotation setting***, we conduct weakly-supervised image-text matching on AdaCL by annotating images with external tools. Specifically, to ensure the generalizability and tool-agnostic nature of AdaCL, we employ four off-the-shelf image

Table 1: Comparisons of image-text matching. Baselines with three types of backbone are compared, i.e., *ResNet+BiGRU:* CMPM (Zhang & Lu, 2018), VSE++(Faghri et al., 2017); *Faster R-CNN+BiGRU:* SCAN(Lee et al., 2018), IMRAM(Chen et al., 2020a), CVSE(Wang et al., 2020a), SGRAFDiao et al. (2021), CHANPan et al. (2023b); *Faster R-CNN+BERT:* DIME(Qu et al., 2021), CHAN(Pan et al., 2023b), CORA(Pham et al., 2024), USER(Zhang et al., 2024).

| Methods | MS-COCO (5-fold 1K) | | | | | | MS-COCO (5K) | | | | | | Flickr30K | | | | | |
|---|---|---|---|---|---|---|---|---|---|---|---|---|---|---|---|---|---|---|
| | Image→Text | | | Text→Image | | | Image→Text | | | Text→Image | | | Image→Text | | | Text→Image | | |
| | R@1 | R@5 | R@10 | R@1 | R@5 | R@10 | R@1 | R@5 | R@10 | R@1 | R@5 | R@10 | R@1 | R@5 | R@10 | R@1 | R@5 | R@10 |
| ***ResNet +BiGRU*** | | | | | | | | | | | | | | | | | | |
| CMPM | 56.1 | 86.3 | 92.9 | 44.6 | 78.8 | 89.0 | 31.1 | 60.7 | 73.9 | 22.9 | 50.2 | 63.8 | 49.6 | 76.8 | 86.1 | 37.3 | 65.7 | 75.5 |
| **AdaCL-CMPM** | **60.7** | **88.2** | **95.0** | **48.5** | **82.8** | **91.4** | **33.9** | **62.3** | **74.4** | **29.1** | **53.3** | **65.5** | **54.7** | **79.0** | **87.5** | **41.6** | **69.4** | **79.2** |
| VSE++ | 64.6 | 90.0 | 95.7 | 52.0 | 84.3 | 92.0 | 41.3 | 71.1 | 81.2 | 30.3 | 59.4 | 72.4 | 52.9 | 80.5 | 87.2 | 39.6 | 70.1 | 79.5 |
| **AdaCL-VSE++** | **65.8** | **91.2** | **96.1** | **54.8** | **85.3** | **93.3** | **44.2** | **72.8** | **83.7** | **33.6** | **61.1** | **73.4** | **55.0** | **84.0** | **87.9** | **44.2** | **73.1** | **81.2** |
| ***Faster R-CNN +BiGRU*** | | | | | | | | | | | | | | | | | | |
| SCAN | 72.7 | 94.8 | 98.4 | 58.8 | 88.4 | 94.8 | 50.4 | 82.2 | 90.0 | 38.6 | 69.3 | 80.4 | 67.4 | 90.3 | 95.8 | 48.6 | 77.7 | 85.2 |
| **AdaCL-SCAN** | **74.3** | **95.4** | **98.5** | **61.2** | **90.1** | **95.5** | **52.2** | **83.6** | **90.9** | **40.6** | **71.7** | **82.2** | **71.4** | **93.0** | **97.2** | **50.9** | **79.9** | **86.8** |
| IMRAM | 76.7 | 95.6 | 98.5 | 61.7 | 89.1 | 95.0 | 53.7 | 83.2 | 91.0 | 39.7 | 69.1 | 79.8 | 74.1 | 93.0 | 96.6 | 53.9 | 79.4 | 87.2 |
| **AdaCL-IMRAM** | **78.3** | **96.3** | **98.5** | **62.5** | **89.8** | **96.0** | **54.3** | **83.8** | **92.3** | **41.4** | **72.3** | **82.6** | **76.1** | **94.3** | **96.9** | **57.2** | **80.8** | **88.1** |
| CVSE | 78.6 | 95.0 | 97.5 | 66.3 | 91.8 | 96.3 | - | - | - | - | - | - | 73.6 | 90.4 | 94.4 | 56.1 | 83.2 | 90.0 |
| **AdaCL-CVSE** | **79.1** | **95.6** | **97.7** | **67.4** | **93.2** | **97.4** | **56.3** | **83.8** | **92.8** | **41.1** | **73.9** | **83.0** | **74.5** | **91.0** | **95.2** | **56.9** | **83.7** | **91.0** |
| SGRAF | 79.6 | 96.2 | 98.5 | 63.2 | 90.7 | 96.1 | 57.8 | - | 91.6 | 41.9 | - | 81.3 | 77.8 | 94.1 | 97.4 | 58.5 | 83.0 | 88.8 |
| **AdaCL-SGRAF** | **80.3** | **96.7** | **98.5** | **64.2** | **91.6** | **96.4** | **56.0** | **85.1** | **92.9** | **42.3** | **74.1** | **82.7** | **78.9** | **95.6** | **97.8** | **58.7** | **83.2** | **89.5** |
| CHAN | 79.7 | 96.7 | 98.7 | 63.8 | 90.4 | 95.8 | 60.2 | 85.9 | 92.4 | 41.7 | 71.5 | 81.7 | 79.7 | 94.5 | 97.3 | 60.2 | 85.3 | 90.7 |
| **AdaCL-CHAN** | **80.9** | **97.1** | **98.7** | **64.7** | **90.6** | **96.0** | **60.7** | **86.4** | **93.4** | **43.0** | **73.3** | **83.0** | **80.8** | **95.1** | **98.0** | **62.1** | **86.0** | **92.3** |
| ***Faster R-CNN +BERT*** | | | | | | | | | | | | | | | | | | |
| DIME | 78.8 | 96.3 | 98.7 | 64.8 | 91.5 | 96.5 | 59.3 | 85.4 | 91.9 | 43.1 | 73.0 | 83.1 | 81.0 | 95.9 | 98.4 | 63.6 | 88.1 | 93.0 |
| **AdaCL-DIME** | **80.3** | **96.7** | **99.0** | **65.5** | **91.7** | **96.9** | **60.0** | **85.7** | **92.2** | **44.3** | **73.6** | **83.8** | **82.6** | **96.3** | **98.9** | **63.6** | **88.4** | **93.7** |
| CHAN | 81.4 | 96.9 | 98.9 | 66.5 | 92.1 | 96.7 | 59.8 | 87.2 | 93.3 | 44.9 | 74.5 | 84.2 | 80.6 | 96.1 | 97.8 | 63.9 | 87.5 | 92.6 |
| **AdaCL-CHAN** | **82.1** | **97.2** | **98.9** | **67.9** | **92.5** | **97.5** | **61.1** | **87.9** | **93.3** | **46.0** | **75.0** | **85.6** | **82.0** | **96.5** | **98.2** | **65.6** | **88.3** | **93.3** |
| CORA | 82.8 | 97.3 | 99.0 | **67.3** | 92.4 | 96.9 | 64.3 | 87.5 | 93.6 | 45.4 | 74.7 | 84.6 | 83.4 | 95.9 | 98.6 | 64.1 | 88.1 | 93.1 |
| **AdaCL-CORA** | **83.3** | **97.3** | **99.2** | 66.9 | **92.6** | **97.2** | **67.2** | **88.8** | **94.2** | **47.4** | **76.1** | **86.6** | **83.9** | **95.9** | **98.6** | **64.7** | **89.1** | **93.6** |
| USER | 83.7 | 96.7 | 99.0 | **67.8** | 91.2 | **95.8** | 67.6 | **88.4** | 93.5 | **47.7** | 75.1 | 83.7 | 86.3 | 97.6 | 99.4 | 69.5 | **91.0** | 94.4 |
| **AdaCL-USER** | **84.9** | **97.1** | **99.1** | 67.6 | **91.5** | 95.7 | **68.1** | 88.2 | **94.1** | 47.3 | **76.7** | **83.7** | **86.4** | **98.2** | **99.4** | **69.9** | 90.8 | **94.6** |

captioning methods (BLIP Li et al. (2022a), GIT Wang et al. (2022b), BLIP-2 Li et al. (2023b), and CoCa Yu et al. (2022)) to generate textual description for images in Flickr30K training set, termed as *pseudo captions*. The expression of pseudo captions is structured and standardized (typically in a subject-verb-object order), which consists of more potential clone negatives. Then we replace the original annotations with pseudo captions and train with AdaCL separately. Despite the fact that some pseudo captions may not perfectly match their corresponding images, we refrain from re-correcting or modifying them, to ensure that the model is trained in a weakly-supervised manner. In this way, AdaCL can be validated on a coarsely annotated dataset, maximizing the resemblance to image-text pairs collected from the Internet. We demonstrate the results of BLIP as image captioning tool in Section 4.3. Due to the page limit, the complete results of GIT, CoCa, BLIP-2, and the format of pseudo captions are detailed in A.1 and A.2 of the appendix.

# 4 Experiments

## 4.1 Setup

**Datasets.** We evaluate AdaCL on two image-text matching datasets, (1) Flickr30K(Young et al., 2014) consists of 31,783 images, each with 5 different sentences. We follow(Lee et al., 2018) to split into training/test/validation of 29,783/1,000/1,000. (2) MS-COCO(Lin et al., 2014) is composed of 123,287 images, each with 5 sentences. We also follow(Lee et al., 2018) to make a training/test/validation of 113,287/5,000/5,000. The test sets are divided into MS-COCO 5-fold 1K (average results of 5 test sets) and MS-COCO 5K (results of 5000 test images).

**Architecture.** For image-text matching, we use three types of backbones: (1) ResNet(He et al., 2016)+BiGRU(Chung et al., 2014), (2) Faster R-CNN(Ren et al., 2015)+BiGRU, and (3) Faster R-CNN+BERT(Devlin et al., 2018). For pre-training, we use CLIP (ViT-B/32), where the embedding size is 512.

**Training Details.** All experiments are performed on four NVIDIA Tesla V100s. For image-text matching, we use a mini-batch size of 64 and the Adam optimizer. The learning rate is 0.0002 and starts decaying 15% of every 10 epochs after epoch 20. The maximum length of each sentence is $a = 32$. For Faster R-CNN, the region number is $n = 36$. The dimension of joint embedding space $D$ is set to 256. We follow (He et al., 2020) to use the momentum memory bank, where the momentum coefficient $z$ is set to 0.99, and the size $M$ is 4096. For AdaCL, $\hat{p}_u$ is set to 0.03, and $\epsilon = e^{-7}$. $m_1$ and $m_2$ are initialized to 20 and 0.1 respectively for adaptive tuning.

**Evaluation Protocols.** Following previous works(Lee et al., 2018), we adopt Recall@K (R@K, K=1, 5, 10) as the evaluation metric. Specifically, given a query text, images are ranked based on their similarity to the query text. A search is considered correct if at least one relevant image appears within the top K positions in the ranking.

### 4.2 Results on Image-text Matching

**Results on image-text matching baselines.** We choose various competitive image-text matching baselines, and the plug-and-play effectiveness of AdaCL, denoted as "AdaCL-Baseline". From Table 1, it is observed that AdaCL outperforms the original baselines across each backbone type. For MS-COCO, AdaCL-CMPM achieves absolute improvement of (4.6%, 1.9%, 2.1%) on (R@1, R@5, R@10) for image-text matching. For Flickr30K, AdaCL-SCAN achieves absolute improvement of (4.0%, 2.7%, 1.4%) and (2.3%, 2.2%, 1.6%) on (R@1, R@5, R@10) for image-text and text-image matching, demonstrating that AdaCL is applicable to a more general network architecture without elaborate cross-modal fusion designing. In A.5 and A.8, we demonstrate the domain generalization capabilities in text-based person retrieval, and efficiency analysis, to better verify its robustness.

**Results on CLIP pre-training.** To assess the scalability of AdaCL, we extend the evaluation to pre-training of widely used contrastive learning framework CLIP, under two specific large-scale datasets Conceptual Caption 3M (CC3M) and 12M (CC12M) (Sharma et al., 2018). We make a fair comparison by training with 32 epochs under the same set of pre-training hyperparameters. We test the zero-shot image-text retrieval performance on Flickr30K and MSCOCO after pre-training. As illustrated in Table 2, AdaCL demonstrates significant improvements under both pre-training data, indicating that AdaCL has great potential in large-scale contrastive learning framework. In A.6 and A.7 of the appendix, we report results of AdaCL in another zero-shot setting on image classification, and more fine-tuning performance of several other vision-language pre-training methods.

Table 2: Zero-shot retrieval on Flickr30K and MSCOCO. "Baseline" and "AdaCL" represent "CLIP+vanilla CL" and "CLIP+AdaCL".

| Data | Methods | Image→Text | | | Text→Image | | |
|---|---|---|---|---|---|---|---|
| | | R@1 | R@5 | R@10 | R@1 | R@5 | R@10 |
| *(Flickr30K)* | | | | | | | |
| CC3M | Baseline | 26.6 | 52.5 | 63.2 | 18.1 | 39.4 | 49.7 |
| | **AdaCL** | 39.5 | 60.8 | 73.7 | 25.5 | 46.9 | 54.3 |
| CC12M | Baseline | 49.3 | 77.3 | 85.0 | 35.5 | 61.8 | 71.6 |
| | **AdaCL** | 51.0 | 77.5 | 87.9 | 38.4 | 64.6 | 74.7 |
| *(MSCOCO)* | | | | | | | |
| CC3M | Baseline | 13.4 | 32.0 | 43.3 | 10.1 | 25.6 | 35.7 |
| | **AdaCL** | 22.5 | 47.1 | 60.7 | 17.8 | 31.6 | 39.5 |
| CC12M | Baseline | 29.3 | 54.4 | 65.3 | 19.0 | 41.0 | 52.5 |
| | **AdaCL** | 34.0 | 55.6 | 65.9 | 25.1 | 47.3 | 57.4 |

Table 3: Effectiveness of AdaCL under weakly-supervised matching (marked by "PC").

| Methods | Image→Text | | | Text→Image | | |
|---|---|---|---|---|---|---|
| | R@1 | R@5 | R@10 | R@1 | R@5 | R@10 |
| AdaCL-CMPM | 54.7 | 79.0 | 87.5 | 41.6 | 69.4 | 79.2 |
| CMPM (PC) | 42.1 | 68.8 | 82.5 | 31.6 | 57.9 | 70.2 |
| **AdaCL-CMPM (PC)** | 46.6 | 73.4 | 85.2 | 34.3 | 63.5 | 74.1 |
| AdaCL-SCAN | 71.4 | 93.0 | 97.2 | 50.9 | 79.9 | 86.8 |
| SCAN (PC) | 55.4 | 80.2 | 90.6 | 36.9 | 69.7 | 81.6 |
| **AdaCL-SCAN (PC)** | 59.7 | 86.3 | 94.6 | 41.4 | 73.6 | 84.0 |
| AdaCL-CVSE | 74.5 | 91.0 | 95.2 | 56.9 | 83.7 | 91.0 |
| CVSE (PC) | 58.0 | 80.4 | 87.8 | 41.5 | 69.4 | 81.3 |
| **AdaCL-CVSE (PC)** | 64.9 | 84.4 | 92.6 | 47.0 | 76.4 | 86.2 |
| AdaCL-DIME | 82.6 | 96.3 | 98.9 | 63.6 | 88.4 | 93.7 |
| DIME (PC) | 62.1 | 86.7 | 93.0 | 44.7 | 72.9 | 84.5 |
| **AdaCL-DIME (PC)** | 70.8 | 88.3 | 93.6 | 48.7 | 81.8 | 90.4 |

Table 4: Study of components. "PC" and "GT" represent trained with pseudo captions (weakly-supervised), and with ground truth annotations.

| | Modules | | | | PC | GT | Image→Text | | Text→Image | |
|---|---|---|---|---|---|---|---|---|---|---|
| | TRL | CL | AdaCL | Anchor | | | R@1 | R@5 | R@1 | R@5 |
| 1 | ✓ | | | | ✓ | - | 51.4 | 77.3 | 40.5 | 66.8 |
| 2 | | ✓ | | | ✓ | - | 43.7 | 69.2 | 31.0 | 64.7 |
| 3 | | | ✓ | | ✓ | - | 57.2 | 82.5 | 41.4 | 73.4 |
| 4 | | | ✓ | ✓ | ✓ | - | 59.6 | 85.2 | 43.1 | 75.6 |
| 5 | ✓ | | | | - | ✓ | 63.8 | 87.0 | 49.1 | 77.3 |
| 6 | | ✓ | | | - | ✓ | 53.7 | 77.0 | 41.3 | 70.4 |
| 7 | | | ✓ | | - | ✓ | 69.0 | 88.4 | 48.8 | 78.0 |
| 8 | | | ✓ | ✓ | - | ✓ | **74.2** | **91.7** | **53.7** | **81.1** |

Table 5: Comparisons of different anchor selection methods.

| **Selection methods** (on $\Delta S$) | Image→Text | | Text→Image | |
|---|---|---|---|---|
| | R@1 | R@5 | R@1 | R@5 |
| Random | 64.2 | 85.9 | 44.5 | 75.1 |
| Maximum | 62.7 | 85.1 | 42.7 | 72.9 |
| Minimum | 71.8 | 90.9 | 50.7 | 79.1 |
| **Ours (Median)** | **74.2** | **91.7** | **53.8** | **81.1** |

### 4.3 Results on Weakly-supervised Image-text Matching with Pseudo Captions

To further validate the applicability of AdaCL in a general annotation setting, we conduct weakly-supervised learning on Flickr30K by replacing the text annotations of the training set with pseudo captions generated by BLIP(Li et al., 2022a). Table 3 demonstrate the performance of AdaCL on several baselines. It can be observed that R@10 of AdaCL (PC) is able to rival the original baselines, indicating that AdaCL effectively distinguishes clone negatives and exhibits strong adaptability to

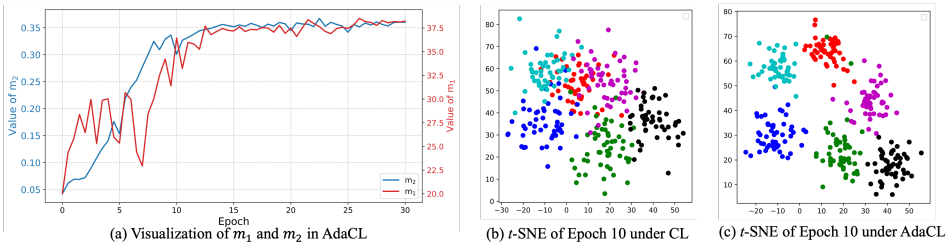


(a) Visualization of $m_1$ and $m_2$ in AdaCL (b) $t$-SNE of Epoch 10 under CL (c) $t$-SNE of Epoch 10 under AdaCL

Figure 3: Analysis of the tuning process and comparison between AdaCL and CL.

automatically annotated text descriptions. The matching capability of AdaCL under an automated annotation setting is in hot pursuit of the fine-grained human annotations, highlighting the potential of AdaCL in weakly-supervised learning. In A.1 of the appendix, we provide additional experiments on other three distinct caption tools to validate AdaCL.

### 4.4 Ablation Study

In this section, we conduct ablation experiments on Flickr30K to verify AdaCL. For fair comparison, we choose Faster R-CNN + BiGRU for feature extractors, and cross attention for alignment learning in all the ablation studies.

**Verification of modules.** In Table 4, we provide detailed verification by setting different learning objectives during training. "AdaCL" in the $3^{rd}$ column refers to employing AdaCL with a random anchor selection method, and "Anchor" in $4^{th}$ column refers to employing both AdaCL and our proposed anchor selection. Meanwhile, two annotation settings, i.e., ground-truth text annotations (GT) and pseudo captions (PC) are compared. The $1^{st}$ to $4^{th}$ rows showcase the results of pseudo captions (weakly-supervised), and $5^{th}$ to $8^{th}$ rows are results based on the ground truth. AdaCL surpasses both TRL and CL across all metrics by a significant margin, proving that AdaCL further facilitates the learning of cross-modal semantics by adaptive tuning. The proposed anchor selection provides AdaCL with absolute R@1 boost of 5.2%(i-t) and 4.9%(t-i). TRL generally exhibits better performance than vanilla CL, suggesting that TRL is supposed to fit in well with retrieval tasks better than vanilla CL. Meanwhile, we also conduct a study of momentum memory bank and mini-batch size. Due to page limit, they are demonstrated in A.9.

**Analysis of anchor selection methods.** To verify the rationality of our proposed anchor selection, we compare with several selection methods. The role of *anchor* is to guide the tuning process of $m_1$ and $m_2$ by propagating the semantic of clone negatives. However, as shown in Table 5, selecting the maximum $\Delta S$ contradicts our motivation since its *anchor* has the lowest likelihood of being representative of clone negatives, which naturally leads to poor matching results. On the contrary, minimum selection aligns well with intuition, while it overlooks the possibility of erroneous reasoning by the model itself. Therefore, an intermediary *anchor*, which reflects the average logit of clone negatives, is proved to be the most effective. In addition, we provide an in-depth analysis of the additional parameters involved in anchor selection methodology in A.10 of the appendix.

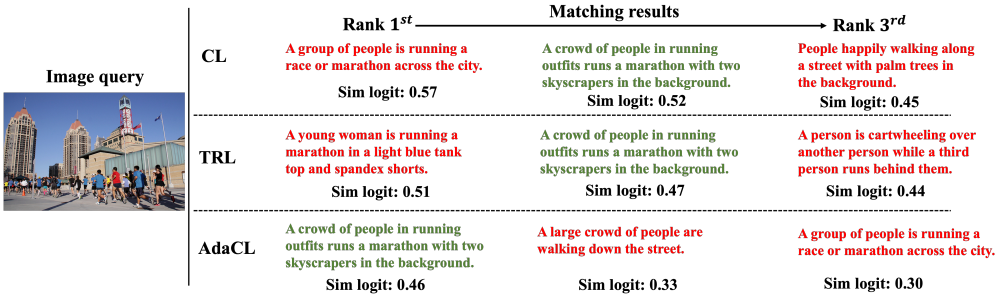


Figure 4: Matching results and similarity logits of clone negatives under CL, TRL, and AdaCL.

**Analysis of adaptive tuning process.** Figure 3(a) illustrates the change of the $m_1$ and $m_2$ in AdaCL. During training, $m_2$ gradually increases and stabilizes around $0.36$, while $m_1$ exhibits some oscillations before reaching a stable value of approximately $38.1$ around Epoch $10$, which exhibits a rapid convergence. Figure 3(b) and (c) showcase the $t$-SNE of the fused embedding in Epoch $10$. AdaCL exhibits a better clustering performance compared to CL, demonstrating its effectiveness in boosting the convergence of the model during training.

### 4.5 Qualitative Analysis and Visualization

**Analysis of clone negatives.** To analyze how AdaCL handles clone negatives, we rank the matching results based on similarity logits and compared three distinct learning objectives. As illustrated in Figure 4, the case study reveals that: (1) AdaCL demonstrates superior R@1 accuracy compared to CL and TRL, successfully eliminating other potential negatives; (2) The representations learned through AdaCL exhibit more discriminative capacity in identifying clone negatives. For instance, the similarity logit for "A group of people running a race or marathon across the city" is merely $0.3$. In contrast, both CL and TRL learn suboptimal similarity logits for clone negatives, despite the presence of the ground-truth text descriptions.

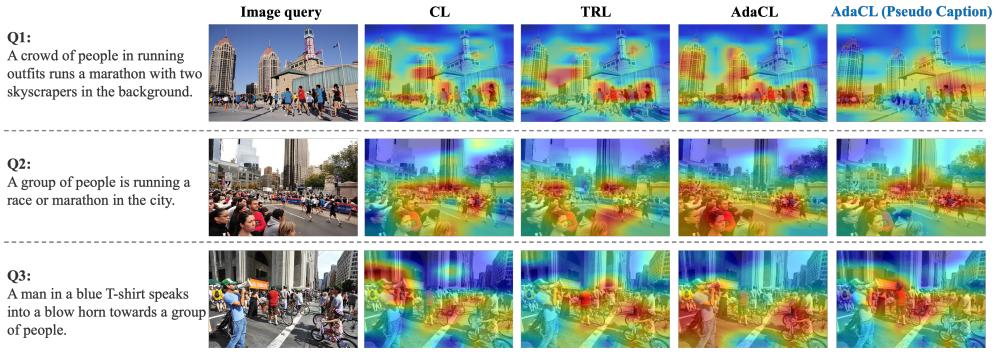


Figure 5: Attention maps in early training stage (Epoch 10). Blue represents AdaCL trained with pseudo captions.

**Visualizations.** We further make qualitative analysis by visualizing several cases in the early training stage to verify the effectiveness of AdaCL in capturing visual cues among clone negatives. It can be observed from Figure 5 that AdaCL are capable of exploring region-level instances together with some background information, such as "two skycrapers" in Q1 and "blow horn" in Q3. Unexpectedly, we find that the distinguishable features among the clone negatives are also learned by AdaCL. For instance, the de facto distinction between Case 2 and Case 1 is the presence of audiences in Case 2. Even though there is no related key word in Q2 such as "audience" or "spectator", AdaCL still precisely captures the spectators in the lower-left corner of the image. Meanwhile, despite the limited textual contents provided by the pseudo captions, AdaCL roughly capture the presence of the crowd in Case 3, whose effectiveness is slightly better than TRL at the same training stage. Please refer to A.11 of the appendix for more visualization and analysis.

## 5 Conclusion

Clone negative is a common but challenging issue in current contrastive learning for image-text matching. To mitigate this, we propose Adaptive Contrastive Learning (AdaCL) that introduces two adaptive margins and a modulating anchor to dynamically adjust the compactness between sample pairs and propagates the semantics of clone negatives. The modulating anchor is selected based on the distribution of negative samples without explicit training, allowing for progressive tuning and enhanced in-batch supervision. Furthermore, We extend AdaCL to a weakly-supervised image-text matching by substituting human-annotated descriptions with automatically generated captions, increasing the number of potential clone negatives. AdaCL demonstrates robustness in both supervised and weakly-supervised image-text matching. Its superiority demonstrates the potential in alleviating the reliance on crowd-sourced annotations and lays a foundation for scalable vision-language contrastive learning.

## REFERENCES


Yi Bin, Haoxuan Li, Yahui Xu, Xing Xu, Yang Yang, and Heng Tao Shen. Unifying two-stream encoders with transformers for cross-modal retrieval. In *Proceedings of the 31st ACM International Conference on Multimedia*, pp. 3041–3050, 2023.

Lukas Bossard, Matthieu Guillaumin, and Luc Van Gool. Food-101–mining discriminative components with random forests. In *Computer vision–ECCV 2014: 13th European conference, zurich, Switzerland, September 6-12, 2014, proceedings, part VI 13*, pp. 446–461. Springer, 2014.

Jane Bromley, Isabelle Guyon, Yann LeCun, Eduard Säckinger, and Roopak Shah. Signature verification using a" siamese" time delay neural network. *Advances in neural information processing systems*, 6, 1993.

Mathilde Caron, Ishan Misra, Julien Mairal, Priya Goyal, Piotr Bojanowski, and Armand Joulin. Unsupervised learning of visual features by contrasting cluster assignments. *Advances in neural information processing systems*, 33:9912–9924, 2020.

Hui Chen, Guiguang Ding, Xudong Liu, Zijia Lin, Ji Liu, and Jungong Han. Imram: Iterative matching with recurrent attention memory for cross-modal image-text retrieval. In *Proceedings of the IEEE/CVF conference on computer vision and pattern recognition*, pp. 12655–12663, 2020a.

Jiacheng Chen, Hexiang Hu, Hao Wu, Yuning Jiang, and Changhu Wang. Learning the best pooling strategy for visual semantic embedding. In *Proceedings of the IEEE/CVF conference on computer vision and pattern recognition*, pp. 15789–15798, 2021.

Ting Chen, Simon Kornblith, Mohammad Norouzi, and Geoffrey Hinton. A simple framework for contrastive learning of visual representations. In *International conference on machine learning*, pp. 1597–1607. PMLR, 2020b.

Yen-Chun Chen, Linjie Li, Licheng Yu, Ahmed El Kholy, Faisal Ahmed, Zhe Gan, Yu Cheng, and Jingjing Liu. Uniter: Universal image-text representation learning. In *European conference on computer vision*, pp. 104–120. Springer, 2020c.

Pengyu Cheng, Weituo Hao, Shuyang Dai, Jiachang Liu, Zhe Gan, and Lawrence Carin. Club: A contrastive log-ratio upper bound of mutual information. In *International conference on machine learning*, pp. 1779–1788. PMLR, 2020.

Yuhao Cheng, Xiaoguang Zhu, Jiuchao Qian, Fei Wen, and Peilin Liu. Cross-modal graph matching network for image-text retrieval. *ACM Transactions on Multimedia Computing, Communications, and Applications (TOMM)*, 18(4):1–23, 2022.

Junyoung Chung, Caglar Gulcehre, KyungHyun Cho, and Yoshua Bengio. Empirical evaluation of gated recurrent neural networks on sequence modeling. *arXiv preprint arXiv:1412.3555*, 2014.

Jia Deng, Wei Dong, Richard Socher, Li-Jia Li, Kai Li, and Li Fei-Fei. Imagenet: A large-scale hierarchical image database. In *2009 IEEE conference on computer vision and pattern recognition*, pp. 248–255. Ieee, 2009.

Jacob Devlin, Ming-Wei Chang, Kenton Lee, and Kristina Toutanova. Bert: Pre-training of deep bidirectional transformers for language understanding. *arXiv preprint arXiv:1810.04805*, 2018.

Haiwen Diao, Ying Zhang, Lin Ma, and Huchuan Lu. Similarity reasoning and filtration for image-text matching. In *Proceedings of the AAAI conference on artificial intelligence*, volume 35, pp. 1218–1226, 2021.

Zefeng Ding, Changxing Ding, Zhiyin Shao, and Dacheng Tao. Semantically self-aligned network for text-to-image part-aware person re-identification. *arXiv preprint arXiv:2107.12666*, 2021.

Fartash Faghri, David J Fleet, Jamie Ryan Kiros, and Sanja Fidler. Vse++: Improving visual-semantic embeddings with hard negatives. *arXiv preprint arXiv:1707.05612*, 2017.

Bo Fang, Wenhao Wu, Chang Liu, Yu Zhou, Yuxin Song, Weiping Wang, Xiangbo Shu, Xiangyang Ji, and Jingdong Wang. Uatvr: Uncertainty-adaptive text-video retrieval. In *Proceedings of the IEEE/CVF International Conference on Computer Vision*, pp. 13723–13733, 2023.

Li Fei-Fei, Rob Fergus, and Pietro Perona. Learning generative visual models from few training examples: An incremental bayesian approach tested on 101 object categories. In *2004 conference on computer vision and pattern recognition workshop*, pp. 178–178. IEEE, 2004.

Jean-Bastien Grill, Florian Strub, Florent Altché, Corentin Tallec, Pierre Richemond, Elena Buchatskaya, Carl Doersch, Bernardo Avila Pires, Zhaohan Guo, Mohammad Gheshlaghi Azar, et al. Bootstrap your own latent-a new approach to self-supervised learning. *Advances in neural information processing systems*, 33:21271–21284, 2020.

Yuanfan Guo, Minghao Xu, Jiawen Li, Bingbing Ni, Xuanyu Zhu, Zhenbang Sun, and Yi Xu. Hcsc: Hierarchical contrastive selective coding. In *Proceedings of the IEEE/CVF Conference on Computer Vision and Pattern Recognition*, pp. 9706–9715, 2022.

Haochen Han, Qinghua Zheng, Guang Dai, Minnan Luo, and Jingdong Wang. Learning to rematch mismatched pairs for robust cross-modal retrieval. In *Proceedings of the IEEE/CVF Conference on Computer Vision and Pattern Recognition*, pp. 26679–26688, 2024.

Kaiming He, Xiangyu Zhang, Shaoqing Ren, and Jian Sun. Deep residual learning for image recognition. In *Proceedings of the IEEE conference on computer vision and pattern recognition*, pp. 770–778, 2016.

Kaiming He, Haoqi Fan, Yuxin Wu, Saining Xie, and Ross Girshick. Momentum contrast for unsupervised visual representation learning. In *Proceedings of the IEEE/CVF conference on computer vision and pattern recognition*, pp. 9729–9738, 2020.

Yan Huang, Yang Long, and Liang Wang. Few-shot image and sentence matching via gated visual-semantic embedding. In *Proceedings of the AAAI conference on artificial intelligence*, volume 33, pp. 8489–8496, 2019.

Zhenyu Huang, Guocheng Niu, Xiao Liu, Wenbiao Ding, Xinyan Xiao, Hua Wu, and Xi Peng. Learning with noisy correspondence for cross-modal matching. *Advances in Neural Information Processing Systems*, 34:29406–29419, 2021.

Ding Jiang and Mang Ye. Cross-modal implicit relation reasoning and aligning for text-to-image person retrieval. In *IEEE International Conference on Computer Vision and Pattern Recognition (CVPR)*, 2023.

Alex Krizhevsky, Geoffrey Hinton, et al. Learning multiple layers of features from tiny images. 2009.

Kuang-Huei Lee, Xi Chen, Gang Hua, Houdong Hu, and Xiaodong He. Stacked cross attention for image-text matching. In *Proceedings of the European conference on computer vision (ECCV)*, pp. 201–216, 2018.

Haoxuan Li, Yi Bin, Junrong Liao, Yang Yang, and Heng Tao Shen. Your negative may not be true negative: Boosting image-text matching with false negative elimination. In *Proceedings of the 31st ACM International Conference on Multimedia*, pp. 924–934, 2023a.

Junnan Li, Ramprasaath Selvaraju, Akhilesh Gotmare, Shafiq Joty, Caiming Xiong, and Steven Chu Hong Hoi. Align before fuse: Vision and language representation learning with momentum distillation. *Advances in neural information processing systems*, 34:9694–9705, 2021.

Junnan Li, Dongxu Li, Caiming Xiong, and Steven Hoi. Blip: Bootstrapping language-image pre-training for unified vision-language understanding and generation. In *International Conference on Machine Learning*, pp. 12888–12900. PMLR, 2022a.

Junnan Li, Dongxu Li, Silvio Savarese, and Steven Hoi. Blip-2: Bootstrapping language-image pre-training with frozen image encoders and large language models. In *International conference on machine learning*, pp. 19730–19742. PMLR, 2023b.

Kunpeng Li, Yulun Zhang, Kai Li, Yuanyuan Li, and Yun Fu. Visual semantic reasoning for image-text matching. In *Proceedings of the IEEE/CVF international conference on computer vision*, pp. 4654–4662, 2019.

Kunpeng Li, Yulun Zhang, Kai Li, Yuanyuan Li, and Yun Fu. Image-text embedding learning via visual and textual semantic reasoning. *IEEE Transactions on Pattern Analysis and Machine Intelligence*, 45(1):641–656, 2022b.

Shuang Li, Tong Xiao, Hongsheng Li, Wei Yang, and Xiaogang Wang. Identity-aware textual-visual matching with latent co-attention. In *Proceedings of the IEEE International Conference on Computer Vision*, pp. 1890–1899, 2017a.

Shuang Li, Tong Xiao, Hongsheng Li, Bolei Zhou, Dayu Yue, and Xiaogang Wang. Person search with natural language description. In *Proceedings of the IEEE conference on computer vision and pattern recognition*, pp. 1970–1979, 2017b.

Xiujun Li, Xi Yin, Chunyuan Li, Pengchuan Zhang, Xiaowei Hu, Lei Zhang, Lijuan Wang, Houdong Hu, Li Dong, Furu Wei, et al. Oscar: Object-semantics aligned pre-training for vision-language tasks. In *Computer Vision–ECCV 2020: 16th European Conference, Glasgow, UK, August 23–28, 2020, Proceedings, Part XXX 16*, pp. 121–137. Springer, 2020.

Zheng Li, Caili Guo, Zerun Feng, Jenq-Neng Hwang, and Zhongtian Du. Integrating language guidance into image-text matching for correcting false negatives. *IEEE Transactions on Multimedia*, 26:103–116, 2023c.

Paul Pu Liang, Zihao Deng, Martin Q Ma, James Y Zou, Louis-Philippe Morency, and Ruslan Salakhutdinov. Factorized contrastive learning: Going beyond multi-view redundancy. *Advances in Neural Information Processing Systems*, 36, 2024.

Tsung-Yi Lin, Michael Maire, Serge Belongie, James Hays, Pietro Perona, Deva Ramanan, Piotr Dollár, and C Lawrence Zitnick. Microsoft coco: Common objects in context. In *Computer Vision–ECCV 2014: 13th European Conference, Zurich, Switzerland, September 6-12, 2014, Proceedings, Part V 13*, pp. 740–755. Springer, 2014.

Chunxiao Liu, Zhendong Mao, Tianzhu Zhang, Hongtao Xie, Bin Wang, and Yongdong Zhang. Graph structured network for image-text matching. In *Proceedings of the IEEE/CVF conference on computer vision and pattern recognition*, pp. 10921–10930, 2020.

Lin Ma, Zhengdong Lu, Lifeng Shang, and Hang Li. Multimodal convolutional neural networks for matching image and sentence. In *Proceedings of the IEEE international conference on computer vision*, pp. 2623–2631, 2015.

Zhuang Ma and Michael Collins. Noise contrastive estimation and negative sampling for conditional models: Consistency and statistical efficiency. *arXiv preprint arXiv:1809.01812*, 2018.

Subhransu Maji, Esa Rahtu, Juho Kannala, Matthew Blaschko, and Andrea Vedaldi. Fine-grained visual classification of aircraft. *arXiv preprint arXiv:1306.5151*, 2013.

Maria-Elena Nilsback and Andrew Zisserman. Automated flower classification over a large number of classes. In *2008 Sixth Indian conference on computer vision, graphics & image processing*, pp. 722–729. IEEE, 2008.

Aaron van den Oord, Yazhe Li, and Oriol Vinyals. Representation learning with contrastive predictive coding. *arXiv preprint arXiv:1807.03748*, 2018.

Renjie Pan, Hua Yang, Cunyan Li, and Jinhai Yang. Joint intra & inter-grained reasoning: A new look into semantic consistency of image-text retrieval. *IEEE Transactions on Multimedia*, 2023a.

Zhengxin Pan, Fangyu Wu, and Bailing Zhang. Fine-grained image-text matching by cross-modal hard aligning network. In *Proceedings of the IEEE/CVF Conference on Computer Vision and Pattern Recognition*, pp. 19275–19284, 2023b.

Omkar M Parkhi, Andrea Vedaldi, Andrew Zisserman, and CV Jawahar. Cats and dogs. In *2012 IEEE conference on computer vision and pattern recognition*, pp. 3498–3505. IEEE, 2012.

Khoi Pham, Chuong Huynh, Ser-Nam Lim, and Abhinav Shrivastava. Composing object relations and attributes for image-text matching. In *Proceedings of the IEEE/CVF Conference on Computer Vision and Pattern Recognition*, pp. 14354–14363, 2024.

Leigang Qu, Meng Liu, Jianlong Wu, Zan Gao, and Liqiang Nie. Dynamic modality interaction modeling for image-text retrieval. In *Proceedings of the 44th International ACM SIGIR Conference on Research and Development in Information Retrieval*, pp. 1104–1113, 2021.

Alec Radford, Jong Wook Kim, Chris Hallacy, Aditya Ramesh, Gabriel Goh, Sandhini Agarwal, Girish Sastry, Amanda Askell, Pamela Mishkin, Jack Clark, et al. Learning transferable visual models from natural language supervision. In *International conference on machine learning*, pp. 8748–8763. PMLR, 2021.

Shaoqing Ren, Kaiming He, Ross Girshick, and Jian Sun. Faster r-cnn: Towards real-time object detection with region proposal networks. *Advances in neural information processing systems*, 28, 2015.

Joshua Robinson, Ching-Yao Chuang, Suvrit Sra, and Stefanie Jegelka. Contrastive learning with hard negative samples. *arXiv preprint arXiv:2010.04592*, 2020.

Florian Schroff, Dmitry Kalenichenko, and James Philbin. Facenet: A unified embedding for face recognition and clustering. In *Proceedings of the IEEE conference on computer vision and pattern recognition*, pp. 815–823, 2015.

Piyush Sharma, Nan Ding, Sebastian Goodman, and Radu Soricut. Conceptual captions: A cleaned, hypernymed, image alt-text dataset for automatic image captioning. In *Proceedings of the 56th Annual Meeting of the Association for Computational Linguistics (Volume 1: Long Papers)*, pp. 2556–2565, 2018.

Botian Shi, Lei Ji, Pan Lu, Zhendong Niu, and Nan Duan. Knowledge aware semantic concept expansion for image-text matching. In *IJCAI*, volume 1, pp. 2, 2019.

Yaniv Taigman, Ming Yang, Marc'Aurelio Ranzato, and Lior Wolf. Deepface: Closing the gap to human-level performance in face verification. In *Proceedings of the IEEE conference on computer vision and pattern recognition*, pp. 1701–1708, 2014.

Haoran Wang, Ying Zhang, Zhong Ji, Yanwei Pang, and Lin Ma. Consensus-aware visual-semantic embedding for image-text matching. In *Computer Vision–ECCV 2020: 16th European Conference, Glasgow, UK, August 23–28, 2020, Proceedings, Part XXIV 16*, pp. 18–34. Springer, 2020a.

Haoran Wang, Dongliang He, Wenhao Wu, Boyang Xia, Min Yang, Fu Li, Yunlong Yu, Zhong Ji, Errui Ding, and Jingdong Wang. Coder: Coupled diversity-sensitive momentum contrastive learning for image-text retrieval. In *European Conference on Computer Vision*, pp. 700–716. Springer, 2022a.

Jian Wang, Feng Zhou, Shilei Wen, Xiao Liu, and Yuanqing Lin. Deep metric learning with angular loss. In *Proceedings of the IEEE international conference on computer vision*, pp. 2593–2601, 2017.

Jianfeng Wang, Zhengyuan Yang, Xiaowei Hu, Linjie Li, Kevin Lin, Zhe Gan, Zicheng Liu, Ce Liu, and Lijuan Wang. Git: A generative image-to-text transformer for vision and language. *arXiv preprint arXiv:2205.14100*, 2022b.

Liwei Wang, Yin Li, Jing Huang, and Svetlana Lazebnik. Learning two-branch neural networks for image-text matching tasks. *IEEE Transactions on Pattern Analysis and Machine Intelligence*, 41 (2):394–407, 2018.

Wenhui Wang, Hangbo Bao, Li Dong, Johan Bjorck, Zhiliang Peng, Qiang Liu, Kriti Aggarwal, Owais Khan Mohammed, Saksham Singhal, Subhojit Som, et al. Image as a foreign language: Beit pretraining for all vision and vision-language tasks. *arXiv preprint arXiv:2208.10442*, 2022c.

Yifei Wang, Qi Zhang, Yaoyu Guo, and Yisen Wang. Non-negative contrastive learning. In *The Twelfth International Conference on Learning Representations*, 2024. URL `https://openreview.net/forum?id=lNCnZwcH5Z`.

Zhe Wang, Zhiyuan Fang, Jun Wang, and Yezhou Yang. Vitaa: Visual-textual attributes alignment in person search by natural language. In *Computer Vision–ECCV 2020: 16th European Conference, Glasgow, UK, August 23–28, 2020, Proceedings, Part XII 16*, pp. 402–420. Springer, 2020b.

Zihao Wang, Xihui Liu, Hongsheng Li, Lu Sheng, Junjie Yan, Xiaogang Wang, and Jing Shao. Camp: Cross-modal adaptive message passing for text-image retrieval. In *Proceedings of the IEEE/CVF international conference on computer vision*, pp. 5764–5773, 2019.

Yiling Wu, Shuhui Wang, Guoli Song, and Qingming Huang. Learning fragment self-attention embeddings for image-text matching. In *Proceedings of the 27th ACM international conference on multimedia*, pp. 2088–2096, 2019.

Mouxing Yang, Yunfan Li, Zhenyu Huang, Zitao Liu, Peng Hu, and Xi Peng. Partially view-aligned representation learning with noise-robust contrastive loss. In *Proceedings of the IEEE/CVF conference on computer vision and pattern recognition*, pp. 1134–1143, 2021.

Peter Young, Alice Lai, Micah Hodosh, and Julia Hockenmaier. From image descriptions to visual denotations: New similarity metrics for semantic inference over event descriptions. *Transactions of the Association for Computational Linguistics*, 2:67–78, 2014.

Jiahui Yu, Zirui Wang, Vijay Vasudevan, Legg Yeung, Mojtaba Seyedhosseini, and Yonghui Wu. Coca: Contrastive captioners are image-text foundation models. *arXiv preprint arXiv:2205.01917*, 2022.

Kun Zhang, Zhendong Mao, Quan Wang, and Yongdong Zhang. Negative-aware attention framework for image-text matching. In *Proceedings of the IEEE/CVF conference on computer vision and pattern recognition*, pp. 15661–15670, 2022.

Pengchuan Zhang, Xiujun Li, Xiaowei Hu, Jianwei Yang, Lei Zhang, Lijuan Wang, Yejin Choi, and Jianfeng Gao. Vinvl: Revisiting visual representations in vision-language models. In *Proceedings of the IEEE/CVF conference on computer vision and pattern recognition*, pp. 5579–5588, 2021.

Yan Zhang, Zhong Ji, Di Wang, Yanwei Pang, and Xuelong Li. User: Unified semantic enhancement with momentum contrast for image-text retrieval. *IEEE Transactions on Image Processing*, 2024.

Ying Zhang and Huchuan Lu. Deep cross-modal projection learning for image-text matching. In *Proceedings of the European conference on computer vision (ECCV)*, pp. 686–701, 2018.

Aichun Zhu, Zijie Wang, Yifeng Li, Xili Wan, Jing Jin, Tian Wang, Fangqiang Hu, and Gang Hua. Dssl: Deep surroundings-person separation learning for text-based person retrieval. In *Proceedings of the 29th ACM international conference on multimedia*, pp. 209–217, 2021.

# A APPENDIX

The appendix is structured as follows:

§A.1 provides experimental results of AdaCL on weakly-supervised image-text matching with pseudo captions generated by three distinct captioning tools GIT, CoCa, and BLIP-2.
§A.2 demonstrates the expression format of pseudo captions generated by four image captioning tools.
§A.3 provides the detailed derivation of the anchor selection proposed in Section 3.4.
§A.4 provides the detailed derivation of Equation 9.
§A.5 provides experimental results of AdaCL on domain generalization (Text-based person retrieval).
§A.6 provides experimental results of AdaCL on zero-shot image classification of CLIP pre-training.
§A.7 provides experimental results of AdaCL on several VLP fine-tuning.
§A.8 provides efficiency analysis of AdaCL.
§A.9 provides ablation study on momentum memory bank and mini-batch sizes.
§A.10 provides an analysis on additional parameters involved in anchor selection.
§A.11 provides a more comprehensive visualization results of clone negatives under CL, TRL, and AdaCL.
§A.12 provides a discussion of the limitations for this work.

## A.1 WEAKLY-SUPERVISED IMAGE-TEXT MATCHING

In the main manuscript, we utilize BLIP(Li et al., 2022a) to generate pseudo captions based on Flickr30K training set. Then, the original text annotations are replaced by the pseudo captions for training to verify the robustness of AdaCL in handling clone negatives. To mitigate concerns about AdaCL's potential reliance on a specific captioning tool, we conduct a range of complementary experiments, to comprehensively analyze its robustness. Specifically, four captioning tools are selected, i.e., GIT(Wang et al., 2022b), CoCa(Yu et al., 2022), and BLIP-2(Li et al., 2023b). GIT is a multi-modal pre-training method that unifies vision-language tasks such as image/video captioning and question answering. CoCa employs a unified transformer architecture to perform both image-text matching and image captioning tasks. CoCa is trained on large-scale image-text pairs and can generate descriptive captions for images while also understanding the relationship between visual and textual content. BLIP-2 is an advanced vision-language model that builds upon its predecessor, BLIP. It introduces a lightweight Querying Transformer (Q-Former) to bridge pre-trained vision and language models efficiently.

In the main manuscript, we obtain pseudo captions through the zero-shot image captioning results of BLIP, same as the way we leverage GIT, CoCa, and BLIP-2. The maximum length of the pseudo caption is 30. Table 6 demonstrates the matching results of different baselines with AdaCL based on pseudo captions. The experimental settings are the same with the settings in the main manuscript.

From Table 6, we can make the following conclusions: By employing different image captioning method, AdaCL demonstrates matching performance that are within a **3%** margin. AdaCL achieves highly competitive performance on the four annotation settings. Therefore, AdaCL is further proved to be applicable to more general annotation settings, where the issue of clone negatives is well mitigated. The impact of image captioning methods on AdaCL is trivial. More specifically, AdaCL-$\mathcal{X}$ (BLIP) and AdaCL-$\mathcal{X}$ (BLIP-2) performs slightly better than AdaCL-$\mathcal{X}$ (GIT) and AdaCL-$\mathcal{X}$ (CoCa). We speculate that this is because the pseudo captions generated by GIT and CoCa typically focus on action and instance information of the image gallery, while the pseudo captions generated by BLIP possess general descriptions, often consisting of a subject-verb-object structure with more holistic-level semantics. Overall, the retrieval performance is quite comparable, further verifying the robustness of AdaCL.

## A.2 EXPRESSION FORMAT OF PSEUDO CAPTIONS

Regarding pseudo captions, we have presented a subset of caption cases generated by four distinct captioning tools (BLIP, GIT, BLIP-2, and CoCa), as illustrated in Figure 6. Pseudo captions generally provide a global and coarse overview of the images, encompassing more potential clone negatives.

Table 6: Comparisons of Image-Text Retrieval performance on Flickr30K test set with pseudo captions generated by four distinct captioning methods. AdaCL-$\mathcal{X}$ (BLIP), AdaCL-$\mathcal{X}$ (GIT), AdaCL-$\mathcal{X}$ (CoCa), and AdaCL-$\mathcal{X}$ (BLIP-2) represent AdaCL with respective image captioning methods. **Bold** is the best performance, while red indicates the margin between the best and worst.

| **Methods** | Image→Text | | | Text→Image | | |
|---|---|---|---|---|---|---|
| | R@1 | R@5 | R@10 | R@1 | R@5 | R@10 |
| AdaCL-CMPM (BLIP) | **46.3** | 72.9 | **85.8** | 34.1 | 63.6 | 75.0 |
| AdaCL-CMPM (GIT) | 44.5 (-1.8) | 71.2 | 84.9 (-0.9) | 32.7 (-1.8) | 61.0 (-2.7) | 73.7 (-1.5) |
| AdaCL-CMPM (CoCa) | 44.8 | 71.0 (-2.4) | 85.1 | 34.1 | **63.7** | 74.6 |
| AdaCL-CMPM (BLIP-2) | 45.9 | **73.4** | 85.7 | **34.5** | 63.3 | **75.2** |
| AdaCL-SCAN (BLIP) | 59.2 | 86.9 | 94.7 | 41.7 | **73.2** | 84.1 |
| AdaCL-SCAN (GIT) | **60.0** | **87.7** | **94.9** | 41.1 | 70.9 (-2.3) | 83.4 (-1.6) |
| AdaCL-SCAN (CoCa) | 58.1 (-1.9) | 85.2 | 94.2 (-0.7) | 40.2 (-2.0) | 72.6 | 83.6 |
| AdaCL-SCAN (BLIP-2) | 58.1 | 85.2 (-2.5) | 94.6 | **42.2** | 74.1 | **85.0** |
| AdaCL-CVSE (BLIP) | 64.7 | 82.6 | **92.9** | **47.0** | 77.5 | 88.4 |
| AdaCL-CVSE (GIT) | 63.6 (-1.9) | 80.9 (-1.8) | 90.9 (-2.0) | 46.2 | 77.4 | **88.7** |
| AdaCL-CVSE (CoCa) | 63.8 | 81.4 | 91.5 | 45.3 (-1.7) | 77.1 (-0.6) | 88.0 (-0.7) |
| AdaCL-CVSE (BLIP-2) | **65.5** | **82.7** | 92.3 | 46.3 | **77.7** | 88.2 |
| AdaCL-DIME (BLIP) | **71.3** | **88.3** | **94.9** | 54.7 | 82.8 | 90.4 |
| AdaCL-DIME (GIT) | 70.1 (-1.2) | 88.0 | 94.2 | 55.1 | 82.3 | 90.6 |
| AdaCL-DIME (CoCa) | 70.8 | 87.8 (-0.5) | 93.7 | 54.6 (-1.3) | 82.0 (-1.4) | 90.0 (-1.0) |
| AdaCL-DIME (BLIP-2) | 70.4 | **88.3** | 93.7 (-1.2) | **55.9** | **83.4** | **91.0** |

Among the four methods, GIT produces the most concise captions, while CoCa tends to generate more detailed descriptions. The weakly-supervised image-text matching based on pseudo captions poses imposes demands for handling clone negatives, thus rendering this task more challenging. We will release all datasets based on pseudo captions to facilitate further research in this domain.

### A.3 Derivation of $m_1$ and $m_2$ in AdaCL

Revisiting AdaCL, **our goal is to progressively tune $m_1$ and $m_2$ based on the *anchor*.** Therefore, we first copy Equation 3 in the main manuscript, i.e., softmax normalized similarity for each image $I$ and its corresponding text $T$ with two margin parameters, which can be expressed as:

$$\hat{p}_i(I) = \frac{\exp\left[m_1(s(I, T_i) - m_2)\right]}{\exp\left[m_1(s(I, T_i) - m_2)\right] + \sum_{j-1, j\neq i}^{M+1} \exp\left[s(I, T_j)\right]}, \tag{12}$$

$$\mathcal{L}_{ada} = \mathbb{E}_{I\sim D}\left[\mathbb{H}(\mathbf{y}(I), \mathbf{p}(I))\right] = -\frac{1}{N}\sum_{i=1}^{N} y_i(I)\log(\hat{p}_i(I)). \tag{13}$$

The potential in-batch clone negatives are represented as:$S^* := \{s \mid p(\mathcal{C} \mid s) > p(\bar{\mathcal{C}} \mid s)\}$, and *anchor* is defined as the median of $S^*$. The two specific boundary functions of the anchor are defined as:

$$\hat{p}_u = \frac{\exp\left[m_1(anchor - m_2)\right]}{\exp\left[m_1(anchor - m_2)\right] + \sum_{anchor}}, \tag{14}$$

$$\frac{\exp\left[m_1(1 - m_2)\right]}{\exp\left[m_1(1 - m_2)\right] + \sum_{anchor}} = 1 - \epsilon, \tag{15}$$

where $\sum_{anchor}$ is the simplification of $\sum_{k=1,k\neq u}^{M+1} \exp\left[s(I_u, T_k)\right]$. $\sum_{anchor}$ can be obtained through Equation 14, expressed as:

$$\sum_{anchor} = \frac{1-\hat{p}_u}{\hat{p}_u} e^{m_1(anchor - m_2)}. \tag{16}$$

| Image Query | Ground-truth Text | BLIP | GIT | BLIP-2 | CoCa |
|---|---|---|---|---|---|
| | A band is playing to a cheering concert with many people. | A crowd of people in a concert with a band on stage. | Many people are enjoying a concert. | A crowd of people in a large concert. | A large crowd of people are gathered in a concert. |
| | Music being played by several individuals while a crowd sits and listens. | People sitting in chairs watching a man play a musical instrument. | People having an indoor concert. | A group of people and a man playing a violin | A group of musicians sitting in a room with instruments . |
| | Two men who are riding on a horse both are trying to rope a bull in a rodeo. | There is a man riding a horse with a cow. | A man riding a horse chasing the cow. | A man is on a horse | A man on a horse roping a calf in a rodeo. |
| | A man wearing blue jeans is trying to stop a horse. | A man is falling off of a horse. | A man is riding a horse. | A man is trying to catch a horse that is running away. | A man in a black and white striped shirt is trying to rope a horse . |
| | A crowded sidewalk in the inner city of an Asian country. | People walking on a street in a city with shops. | People walking on the street. | A group of people walking down a street | A group of people walking down a street . |
| | A crowd of people is walking down the middle of a city street. | There are many people walking down the street together. | Many people gather on the street. | A large crowd of people walking down a street. | A crowd of people walking down a street . |
| | A crowd of people in running outfits runs a marathon with two skyscrapers in the background. | People running in a marathon in a city with tall buildings. | People are jogging during the day. | A group of people running in a city | A group of people walking on the sidewalk near a building . |
| | A group of people is running a race or marathon in the city. | People are running in a marathon in a city street | Athletes running in the city. | A large crowd of people running in a marathon | A group of people that are standing in the street . |
| | A man in a blue T-shirt speaks into a blow horn towards a group of people. | People are walking in a crowded city street. | Cyclists riding across the street. | A man is standing on a street corner with a megaphone | A group of people riding bikes down a street . |
| | Many people are chilling in front an old building. | People are in front of a large building with a clock tower. | Tourists sitting at tables outside the building. | A crowd of people sitting at tables outside of a building. | A crowd of people sitting at tables in front of a building. |
| | A group of people stand in the park of a city, with buildings in the background. | People standing around a fountain in a city with tall buildings | Several people are standing in the park. | A group of people standing in the park. | A group of people standing in front of a water fountain . |

Figure 6: Cases of pseudo captions by four distinct captioning tools, i.e., BLIP, GIT, BLIP-2, and CoCa.

Combining Equation 16 and Equation 15, we have:

$$\left[e^{m_1(1-m_2)} + \frac{1-\hat{p}_u}{\hat{p}_u} e^{m_1(anchor-m_2)}\right](1-\epsilon) = e^{m_1(1-m_2)}. \tag{17}$$

To simplify Equation 17, we have:

$$\frac{(1-\epsilon)(1-\hat{p}_u)}{\hat{p}_u} e^{m_1 \cdot anchor} = \epsilon \cdot e^{m_1}. \tag{18}$$

By taking the logarithm of both sides of Equation 18, we have:

$$m_1 \cdot anchor + log \frac{(1-\epsilon)(1-\hat{p}_u)}{\hat{p}_u} = m_1 + log\ \epsilon. \tag{19}$$

Then, $m_1$ can be obtained, expressed as:

$$m_1 = log(\frac{\epsilon\ \hat{p}_u}{(1-\epsilon)(1-\hat{p}_u)})/(anchor - 1), \tag{20}$$

which corresponds to Algorithm 1 in the manuscript. Meanwhile, by taking the logarithm of both sides of Equation 16, we have:

$$log \sum_{anchor} = log \frac{1-\hat{p}_u}{\hat{p}_u} + m_1(anchor - m_2). \tag{21}$$

Simplifying Equation 21, we obtain $m_2$:

$$m_2 = anchor + log(\frac{1-\hat{p}_u}{\hat{p}_u \cdot \sum_{anchor}})/m_1, \tag{22}$$

which corresponds to Algorithm 1 in the main manuscript. With Equation 20 and Equation 22, $m_1$ and $m_2$ can be computed and updated during each batch training process with the supervision of *anchor*, facilitating the model to exploit more distinguishable cross-modal semantics among samples compared with the original TRL and CL.

### A.4 Derivation of Equation 9

The derivation of Equation 9 in the manuscript. To begin with, the $K$-class classification probability with Bayes's formula can be expressed as:

$$p(y=i \mid x) = \frac{p(x \mid y=i)p(y=i)}{\sum_{j=1}^{K} p(x \mid y=j)p(y=j)} = \frac{\exp\left(f_i(x)\right)}{\sum_{j=1}^{K} \exp\left(f_j(x)\right)}, \tag{23}$$

In anchor selection of AdaCL, the input variable $x$ (a.k.a $s$) is one-dimensional with a binary output variable $y \in 0, 1$ (a.k.a $\bar{\mathcal{C}}$ and $\mathcal{C}$). We aim to predict $p(y=1 \mid x)$. Gaussian Discriminant Analysis (GDA) assumes that for each class $y=0$ and $y=1$, the input $x$ follows a Gaussian distribution. This can be expressed as: $p(x \mid y=0) = \mathcal{N}\left(x \mid \mu_0, \sigma_0^2\right)$ and $p(x \mid y=1) = \mathcal{N}\left(x \mid \mu_1, \sigma_1^2\right)$. $\mu_0$, $\mu_1$ and $\sigma_0^2$, $\sigma_1^2$ are the means and variances of distributions for classes $y=0$ and $y=1$, respectively. Thus, the posterior probability can be expressed as:

$$p(y=0 \mid x) = \frac{\mathcal{N}\left(x \mid \mu_0, \sigma_0^2\right) \cdot \pi_0}{\mathcal{N}\left(x \mid \mu_0, \sigma_0^2\right) \cdot \pi_0 + \mathcal{N}\left(x \mid \mu_1, \sigma_1^2\right) \cdot \pi_1}, \tag{24}$$

$$p(y=1 \mid x) = \frac{\mathcal{N}\left(x \mid \mu_1, \sigma_1^2\right) \cdot \pi_1}{\mathcal{N}\left(x \mid \mu_1, \sigma_1^2\right) \cdot \pi_1 + \mathcal{N}\left(x \mid \mu_0, \sigma_0^2\right) \cdot \pi_0}. \tag{25}$$

Since $\mathcal{N}\left(x \mid \mu_1, \sigma_1^2\right)$ is the probability density function of a Gaussian distribution, we substitute $\mathcal{N}\left(x \mid \mu_1, \sigma_1^2\right) = \frac{1}{\sqrt{2\pi\sigma^2}} \exp\left(-\frac{(x-\mu)^2}{2\sigma^2}\right)$ into the above equations, obtaining Eqation 9 in the manuscript:

$$p\left(y=0 \mid x\right) = \frac{1}{1 + \frac{\pi_1}{\pi_0}\frac{\sigma_0}{\sigma_1} \exp\left[\frac{(s-\mu_0)^2}{2\sigma_0^2} - \frac{(s-\mu_1)^2}{2\sigma_1^2}\right]}, \tag{26}$$

$$p\left(y=1 \mid x\right) = \frac{1}{1 + \frac{\pi_0}{\pi_1}\frac{\sigma_1}{\sigma_0} \exp\left[\frac{(s-\mu_1)^2}{2\sigma_1^2} - \frac{(s-\mu_0)^2}{2\sigma_0^2}\right]}, \tag{27}$$

$p\left(y=0 \mid x\right)$ and $p\left(y=1 \mid x\right)$ represent the probability of a similarity score to be a clone negative or not, without the need of explicit pre-processing to the dataset or training.

Table 7: R@1 Results on text-based person search. "DG" stands for domain generalization, and "FT" for fine-tuning on the corresponding dataset.

| Method | CUHK-PEDES | | ICFG-PEDES | | RSTPReid | |
|---|---|---|---|---|---|---|
| | DG | FT | DG | FT | DG | FT |
| CL | 16.3 | 49.3 | 15.8 | 43.5 | 12.7 | 30.1 |
| **AdaCL** | **30.5** | **56.7** | **27.9** | **49.0** | **23.9** | **41.4** |

### A.5 Domain Generalization on Text-based Person Retrieval

To evaluate the robustness of AdaCL as a plug-and-play module, we seek to evaluate its domain generalization capabilities in the context of text-based person retrieval. Specifically, we conduct training using Flickr30K and select three mainstream text-based person retrieval datasets, CUHK-PEDES(Li et al., 2017b), ICFG-PEDES(Ding et al., 2021), and RSTPReid(Zhu et al., 2021) for domain generalization experiments. To ensure a fair comparison, we choose CMPM as the baseline, as the learning objective it adopt in its paper is the closest to vanilla contrastive loss, and its original paper conducted experiments on two of the datasets. The result on RSTPReid is evaluated by us with CMPM's official repository. As illustrated in Table 7, it is observed that AdaCL boosts CMPM by a large margin. Especially for DG, the results of AdaCL on each dataset improves by over 10%.

Table 8: Fine-tuning results of AdaCL on three baselines under ICFG-PEDES.

| Method | Text-Image R@1 | Text-Image R@5 | Text-Image R@10 |
|---|---|---|---|
| CMPM | 43.5 | 65.4 | 74.2 |
| **AdaCL-CMPM** | **49.0** | **69.7** | **79.1** |
| ViTAA | 51.0 | 68.8 | 75.8 |
| **AdaCL-ViTAA** | **54.8** | **74.1** | **78.6** |
| IRRA | 63.5 | 80.3 | 85.8 |
| **AdaCL-IRRA** | **64.3** | **81.1** | **86.5** |

Table 9: Fine-tuning results of AdaCL on three baselines under RSTPReid.

| Method | Text-Image R@1 | Text-Image R@5 | Text-Image R@10 |
|---|---|---|---|
| CMPM | 30.1 | 38.5 | 59.6 |
| **AdaCL-CMPM** | **41.4** | **57.0** | **55.7** |
| ViTAA | 37.7 | 60.6 | 66.5 |
| **AdaCL-ViTAA** | **42.6** | **62.1** | **69.2** |
| IRRA | 60.2 | 81.3 | 88.2 |
| **AdaCL-IRRA** | **62.7** | **81.4** | **89.0** |

For fine-tuning, in addition to CUHK-PEDES, we also validate the performance of AdaCL on ICFG-PEDES and RSTPReid. We employ three baselines: CMPM(Zhang & Lu, 2018), ViTAA(Wang et al., 2020b), and IRRA(Jiang & Ye, 2023), and compare the effectiveness of incorporating AdaCL as a constraint. The experimental results w/ and w/o using AdaCL are presented in Table 8 and Table 9. It can be observed that AdaCL demonstrates significant improvements across all three baselines, achieving enhancements of 5.5%, 3.8%, and 0.8% in R@1, respectively. These matching results substantiate the robustness of AdaCL in other cross-modal tasks, demonstrating its insensitivity to the diverse dataset distributions (both natural images and person search images), and the choice of baselines.

### A.6 Zero-shot Image Classification of AdaCL in CLIP pre-training

In addition to image-text matching, we also evaluate AdaCL on other pre-training task, i.e., zero-shot image classification. Specifically, we validate AdaCL on eight common classification benchmarks,

which can be divided into (i) general datasets: ImageNet(Deng et al., 2009), CIFAR-10(Krizhevsky et al., 2009), CIFAR-100(Krizhevsky et al., 2009), Caltech-101(Fei-Fei et al., 2004)), and (ii) fine-grained datasets: Food-101(Bossard et al., 2014), Flowers-102(Nilsback & Zisserman, 2008), OxfordPets(Parkhi et al., 2012), and FGVCAircraft(Maji et al., 2013). The Top-1 accuracy results of "CLIP + AdaCL" pretrained on CC3M and CC12M are demonstrated in Table 10:

Table 10: Zero-shot image classification of CLIP pre-training under different learning objectives. "Baseline" represents "CLIP+vanilla contrastive learning", and "AdaCL" represents "CLIP+AdaCL". Results under two pre-training settings, i.e., CC3M and CC12M are compared.

| **Data** | **Model** | **Datasets** | | | | | | | |
|---|---|---|---|---|---|---|---|---|---|
| | | ImageNet | CIFAR-10 | CIFAR-100 | Caltech-101 | Food-101 | Flowers | Pets | Aircraft |
| CC3M | Baseline | 17.2 | 71.3 | 32.1 | 50.9 | 10.2 | 10.8 | 12.1 | 1.0 |
| | **AdaCL** | **22.0** | **77.1** | **42.2** | **54.8** | **12.6** | **13.3** | **14.9** | **1.7** |
| CC12M | Baseline | 32.9 | 72.5 | 38.0 | 74.0 | 26.5 | **25.7** | 46.2 | 2.6 |
| | **AdaCL** | **34.8** | **73.4** | **43.3** | **74.7** | **33.1** | 25.4 | **46.7** | **2.8** |

It is observed that AdaCL outperforms CL in all the general datasets and most of the fine-grained datasets, proving its advantage in recognition tasks. Specifically, in ImageNet, CIFAR-10, CIFAR-100, the Top-1 accuracy of AdaCL has surpassed vanilla CL by over 5%. It is noteworthy that the performance on fine-grained datasets further verifies AdaCL's capacity in challenging scenarios.

### A.7 VLP Fine-tuning

Apart from CLIP pre-training, we want to further assess the fine-tuning results of AdaCL in several other Vision Language Pre-training methods (VLP). Therefore we extend the evaluation to a range of open-source VLPs by fine-tuning using AdaCL on MS-COCO (5K), and remain the original experimental settings. As illustrated in Table 11, AdaCL demonstrates significant improvements across nearly all metrics under both dual-encoder method (BEIT-3(Wang et al., 2022c)) and fusion-encoder methods (UNITER(Chen et al., 2020c), OSCAR(Li et al., 2020), VinVL(Zhang et al., 2021)), effectively boosting the fine-tuning process. These results further corroborate the robustness of AdaCL across multiple baselines.

Table 11: Results of AdaCL on VLP fine-tuning.

| **Methods** | Image→Text | | | Text→Image | | |
|---|---|---|---|---|---|---|
| | R@1 | R@5 | R@10 | R@1 | R@5 | R@10 |
| UNITER† | 65.7 | 88.6 | 93.8 | 52.9 | 79.9 | 88.0 |
| **AdaCL-UNITER** | **67.6** | **89.0** | **94.3** | **55.1** | **81.2** | **88.9** |
| OSCAR | 70.0 | 91.1 | 95.5 | 54.0 | 80.8 | 88.5 |
| **AdaCL-OSCAR** | **71.0** | **92.7** | **96.3** | **54.0** | 80.6 | **89.1** |
| VinVL | 75.4 | 92.9 | 96.2 | 58.8 | 83.5 | 90.3 |
| **AdaCL-VinVL** | **78.7** | **94.4** | **96.8** | **60.4** | **84.2** | **91.1** |
| BEIT-3 | 84.8 | 96.5 | 98.3 | 67.2 | 87.7 | 92.8 |
| **AdaCL-BEIT-3** | 84.4 | **96.9** | 98.3 | **68.6** | **89.1** | **93.7** |

† Evaluated by us with official repository.

### A.8 EFFICIENCY ANALYSIS

Serving as a plug-and-play module, AdaCL does not increase the inference time since it is independent of the cross-modal reasoning module. For training efficiency, we add detailed analysis on AdaCL. The speed of model convergence mirrors the learning efficiency of a certain constraint. As shown in Figure 7, AdaCL brings considerable convergence efficiency and retrieval results, which even boost CMPM and DIME to achieve their ultimate results within the first 5 epochs, demonstrating the scalability and efficiency of AdaCL.

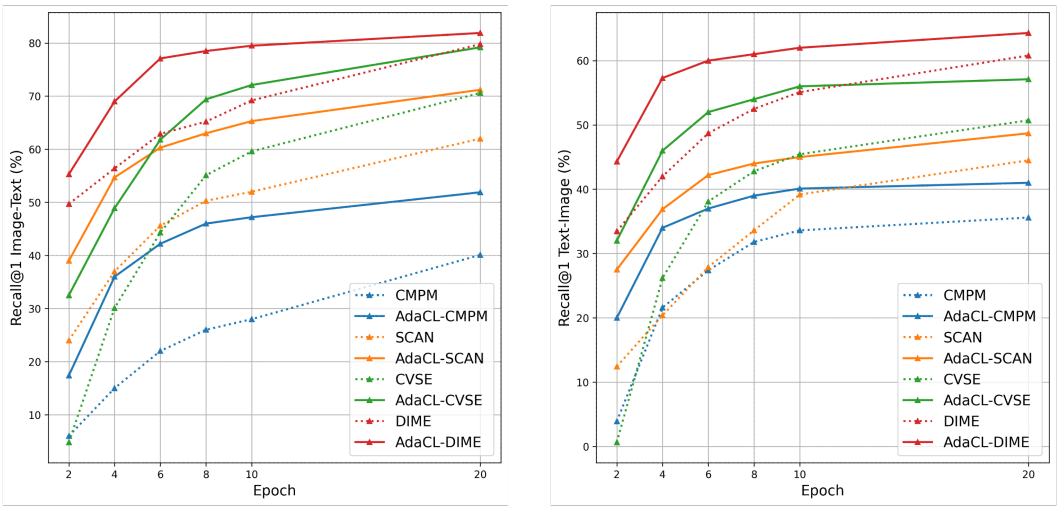


(a) Convergence efficiency of Image-text retrieval (b) Convergence efficiency of Text-image retrieval

Figure 7: Training efficiency of AdaCL.

### A.9 EXPERIMENTS ON MOMENTUM MEMORY BANK AND MINI-BATCH SIZE

**Analysis of momentum memory bank.** Since memory bank is widely adopted in vision-language contrastive learning, we further analyze AdaCL by varying the memory bank size $M$, which leads to different number of negative samples. The results in Table 12 reveal that the momentum memory bank yields a modest yet discernible improvement: Among the sizes of $4096$, $6144$, and $8192$, the impact of memory bank is not that significant. This suggests that AdaCL does not excessively rely on the quantity of negative samples for an ideal similarity distribution.

Table 12: Effect of different memory bank sizes.

| **Memory Bank Size** | Image→Text | | | Text→Image | | |
|---|---|---|---|---|---|---|
| | R@1 | R@5 | R@10 | R@1 | R@5 | R@10 |
| N/A | 70.3 | 90.0 | 95.5 | 49.5 | 77.5 | 87.3 |
| 2048 | 71.9 | 90.9 | 96.7 | 51.4 | 78.4 | 87.3 |
| 4096 | **74.2** | 91.7 | 97.9 | **53.7** | 81.1 | **88.2** |
| 6144 | 73.7 | **91.9** | **98.2** | 53.2 | 79.6 | 87.8 |
| 8192 | 73.9 | 91.4 | 98.0 | 53.3 | **80.5** | 87.8 |

**Analysis of mini-batch size.** Since mini-batch size is correlated with the number of potential anchor candidates for selection, we also investigate the impact of mini-batch size, as shown in Table 13. It can be observed that AdaCL exhibits remarkable robustness to variations in batch size settings. Across a range of batch sizes from 16 to 128, the fluctuation in R@1 remains within a narrow margin of 4%.

Table 13: Effect of different mini-batch sizes.

| **Batch Size** | Image→Text | | | Text→Image | | |
|---|---|---|---|---|---|---|
| | R@1 | R@5 | R@10 | R@1 | R@5 | R@10 |
| 16 | 70.6 | 89.2 | 96.5 | 50.0 | 79.3 | 84.8 |
| 32 | 72.9 | 90.9 | 97.4 | 52.1 | 81.0 | 87.1 |
| 64 | **74.2** | **91.7** | **97.9** | 53.7 | 81.1 | **88.2** |
| 128 | 74.0 | 91.2 | 97.6 | **53.9** | **81.2** | 88.0 |

### A.10 Additional parameters in anchor selection

Here we further analyze the anchor selection methodology. In the main manuscript, we utilize the negatives from $S_{sln}$ and $S_{cln}$ within each mini-batch to represent the empirical means and variances. However, since we cannot guarantee that all samples in $S_{sln}$ and $S_{cln}$ are exclusively salient negatives and clone negatives, respectively. Based on this speculation, we continue to select Top-$K$ similarity scores from $S_{sln}$ and $S_{cln}$ as observational samples for calculating means and variances. We do this because higher similarity scores for certain negatives correlate with an increased probability of them being clone negatives. We set $K$ to 32 and conduct experiments on CMPM, SCAN, and DIME under Flickr30K, as shown in Table 14. It can be concluded that employing Top-$K$ selection strategy does not result in a significant improvement or deterioration in matching performance, with fluctuations generally remaining within a 2% range. This observation contradicts our initial hypothesis and intuition. Consequently, we can infer that AdaCL exhibits ***low sensitivity to the specific values of the empirical mean and variance***, which is another minor merit of AdaCL. Given that the Top-$K$ selection explicitly increase computation without yielding significant performance improvements, we have opted to maintain the original calculation method in the main manuscript.

Table 14: Matching results of Top-$K$ selection for empirical means and variances.

| **Methods** | Image→Text | | | Text→Image | | |
|---|---|---|---|---|---|---|
| | R@1 | R@5 | R@10 | R@1 | R@5 | R@10 |
| AdaCL-CMPM | 54.7 | 79.0 | 87.5 | 41.6 | 69.4 | 79.2 |
| AdaCL-CMPM † | 54.2 | 77.8 | 87.1 | 41.8 | 68.1 | 80.0 |
| AdaCL-SCAN | 71.4 | 93.0 | 97.2 | 50.9 | 79.9 | 86.8 |
| AdaCL-SCAN † | 72.7 | 93.4 | 96.5 | 50.2 | 79.0 | 87.1 |
| AdaCL-DIME | 82.6 | 96.3 | 98.9 | 63.6 | 88.4 | 93.7 |
| AdaCL-DIME † | 82.4 | 95.3 | 98.7 | 63.7 | 88.2 | 93.0 |

† Employ Top-$K$ selection.

### A.11 More Visualization of AdaCL

We present a more comprehensive comparison of CL, TRL, and AdaCL trained with ground-truth annotations and pseudo captions. The visualization results of the early training stage are demonstrated in Figure 8, which include 4 kinds of clone negatives with 11 cases. Based on the attention maps, we can summarize the following conclusions: AdaCL captures abundant semantics on highly similar clone negatives. Specifically, case (a) and case (b) demonstrate that AdaCL boosts the exploration of spatial semantics among the images, such as "music being played by several individuals", as well as "is trying to stop a horse", which effectively distinguishes clone negatives apart. Additionally, case (c) demonstrates AdaCL's ability in capturing background information such as "Asian country" and "a city street" are crucial phrases that are reasoned through AdaCL. Case (d) showcases five examples of urban landscape, demonstrating that AdaCL is able to discover instances that are not explicitly described in the text query. For instance, the unique attribute "spectator" is not included in Q8, but AdaCL facilitate learning the corresponding representation, which is highlighted in the attention map.

Also, the latent "fountain" is not included in Q11 but reasoned by AdaCL. In this way, AdaCL is proved to achieve comprehensive cross-modal semantics with its adaptive tuning strategy even when the quality of textual annotations is not high. This finding presents great potential of AdaCL to handle retrieval with low quality labels.

Furthermore, we obtain the attention maps by training with pseudo captions under AdaCL, as depicted in the last column of Figure 8. Due to the lack of instance-level information during the training process, we do not expect the results to surpass models trained on original annotations. However, AdaCL (Pseudo Caption) manages to capture the approximate cross-modal semantics and pays attention to the fine-grained representation, which outperforms CL and TRL (trained with ground-truth) in most cases. This demonstrates the prospects of AdaCL in the vision-language contrastive learning of automatically annotated image-text pairs.

### A.12 Discussion: Limitation

In this work, AdaCL is evaluated on (1) image-text matching under Flickr30K, MS-COCO, (2) CLIP pre-training under CC3M and CC12M, (3) weakly-supervised image-text matching under pseudo captions, (4) text-based person search under CUHK-PEDES, ICFG-PEDES, and RSTPReid. We have not extended AdaCL to an all-round vision-language tasks due to time and computational limitations, which is undoubtedly planned in our future endeavor.

Also, although AdaCL maintains high convergence efficiency, we acknowledge that AdaCL introduces additional components, which may increase the computation during training. AdaCL introduces a moderate computational overhead of $O(N\dot{M})$ per batch training, and we believe this trade-off is acceptable given the context of contrastive learning and pre-training. In future work, we will delve into a more lightweight architecture of adaptive contrastive learning method.

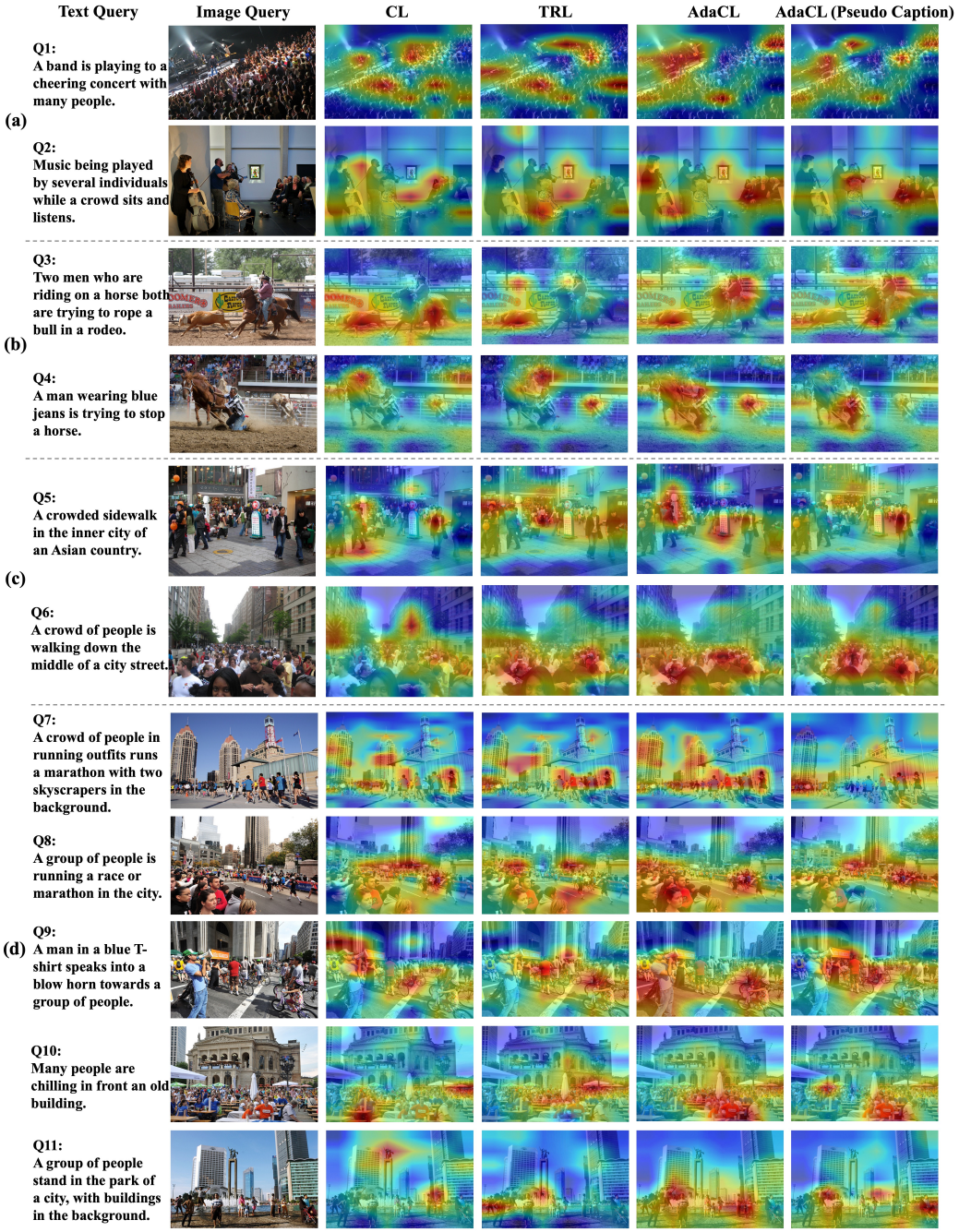


Figure 8: Attention maps of clone negative cases in early stage (Epoch 10). “CL”, “TRL”, and “AdaCL” represent model trained with different constraints, i.e., Contrasive Learning, Triplet Ranking Loss, and the proposed Adaptive Contrasive Learning. Blue represents AdaCL trained with pseudo captions.